

Annihilation vs. Decay: Constraining dark matter properties from a gamma-ray detection

Sergio Palomares-Ruiz

Centro de Física Teórica de Partículas, Instituto Superior Técnico,
Av. Rovisco Pais 1, 1049-001 Lisboa, Portugal

E-mail: sergio.palomares.ruiz@ist.utl.pt

Jennifer M. Siegal-Gaskins

Center for Cosmology and Astro-Particle Physics, The Ohio State University,
191 W. Woodruff Ave., Columbus, OH 43210, USA

E-mail: jsg@mps.ohio-state.edu

Abstract. Most proposed dark matter candidates are stable and are produced thermally in the early Universe. However, there is also the possibility of unstable (but long-lived) dark matter, produced thermally or otherwise. We propose a strategy to distinguish between dark matter annihilation and/or decay in the case that a clear signal is detected in gamma-ray observations of Milky Way dwarf spheroidal galaxies with gamma-ray experiments. The sole measurement of the energy spectrum of an indirect signal would render the discrimination between these cases impossible. We show that by examining the dependence of the intensity and energy spectrum on the angular distribution of the emission, the origin could be identified as decay, annihilation, or both. In addition, once the type of signal is established, we show how these measurements could help to extract information about the dark matter properties, including mass, annihilation cross section, lifetime, dominant annihilation and decay channels, and the presence of substructure. Although an application of the approach presented here would likely be feasible with current experiments only for very optimistic dark matter scenarios, the improved sensitivity of upcoming experiments could enable this technique to be used to study a wider range of dark matter models.

Keywords: dark matter theory, gamma-ray theory, dwarf galaxies

PACS numbers: 95.35.+d, 95.85.Pw, 98.56.Wm, 98.62.Gq

CFTP/10-003

Submitted to: *Journal of Cosmology and Astroparticle Physics*

1. Introduction

Many different astrophysical and cosmological observations have found evidence for the existence of non-luminous, non-baryonic dark matter (for reviews see, e.g., Refs. [1–3]) and indicate that it constitutes about 80% of the mass content of the Universe [4]. Despite the precision with which the cosmological dark matter density has been measured, little is known about the origin and properties of the dark matter particle, such as its mass, spin, couplings, and its distribution on small scales.

Several candidate dark matter particles have been proposed with masses from the electroweak scale to superheavy candidates at the Planck scale (see, e.g., Refs. [3, 5] for a comprehensive list). Light particles have also been considered as possible dark matter candidates: axions [6], sterile neutrinos with masses in the keV range [7] and light scalars with MeV–GeV masses [8–11]. However, the most popular candidates are weakly interacting massive particles (WIMPs) which arise in extensions of the Standard Model such as supersymmetric (e.g., Ref. [1]), little Higgs (e.g., Ref. [12]), or extra-dimensions models (e.g., Ref. [13]).

Most proposed WIMPs are stable and are produced thermally in the early Universe with an annihilation cross section (times relative velocity) of $\langle\sigma v\rangle \sim 3 \times 10^{-26} \text{ cm}^3 \text{ s}^{-1}$. However, dark matter may be unstable but long-lived; the only requirement in order for it to be a thermal relic and present today is that it has a lifetime τ_χ much longer than the age of the Universe $t_U \simeq 4 \times 10^{17} \text{ s}$. It is also possible that dark matter is not a thermal relic, which would allow it to have a larger annihilation cross section than the canonical value for WIMP thermal relics.

Although the case of a non-thermal [14, 15] or unstable [16] dark matter candidate was considered several decades ago, recently a great deal of interest in these scenarios has been generated by the rise in the positron fraction in the tens of GeV range measured by the PAMELA experiment [17]. One possibility to explain the PAMELA data is by the injection of positrons by annihilation [18–21], decay [22, 23] or both [24] of dark matter in the solar neighborhood (see also Ref. [25] and references therein). In the case of annihilation in the smooth halo, enhancements to the annihilation cross-section of the order of $10\text{--}10^5$ are required (with respect to thermal dark matter with no Sommerfeld or Breit-Wigner enhancements and assuming there is no nearby dark matter clump) [18]. However, note that the contribution from substructure could be significant [26] and interestingly, the cumulative effect from distant subhalos could modify the electron and positron spectra at our galactic position [27].

Indirect dark matter searches look for the products of dark matter annihilation or decay, which include not only antimatter, as in the case of PAMELA, but also neutrinos [28, 29] and photons. In particular, targets for indirect searches in gamma-rays include dark matter in extragalactic structures [30], the Galactic Center [31–34], the Milky Way halo [34–37], its subhalos [34, 36, 38, 39] and known dwarf galaxies [34, 40–48].

Different approaches have been proposed to constrain dark matter properties by using indirect or direct measurements or their combination [49–53]. To extract the

properties of the dark matter particle from the detection of an indirect signal requires several pieces of information. While the energy spectrum of the signal is dependent on the dark matter properties (mass m_χ , annihilation cross section $\langle\sigma v\rangle$, lifetime τ_χ , and annihilation and/or decay channels), sufficient degeneracies exist to prevent accurate reconstruction of the dark matter properties from the energy spectrum alone. In particular, the sole measurement of the energy spectrum would make it impossible to know if the indirect signal from dark matter is produced by annihilation or decay. The spectrum of the former is characterized by a cutoff at an energy equal to the dark matter mass, while the cutoff in the spectrum from the latter is at an energy equal to half of the dark matter mass.

In this work we address the following two questions: (1) in the case that an indirect dark matter signal is detected in gamma rays, can annihilation and/or decay be identified as the origin of the signal? and (2) what information about the particle properties can be obtained from the indirect measurement? If dark matter is unstable and produces an observable signal from decay, an annihilation signal may also be present. In principle, there is a range of parameters for which the two signals would be comparable, which would present a challenge for distinguishing the cases of annihilation, decay, and those where both annihilation and decay are significant contributors to the measured signal.

In order to tackle this problem, we propose a strategy to distinguish between these scenarios using gamma-ray observations of Milky Way dwarf spheroidal galaxies with current or future gamma-ray telescopes. Current missions include the Large Area Telescope (LAT) aboard the Fermi Gamma-ray Space Telescope (*Fermi*) [54], which observes gamma-rays in the range from 20 MeV to greater than 300 GeV, and atmospheric Čerenkov telescopes (ACTs) such as HESS [55], VERITAS [56], and MAGIC [57], which observe emission above ~ 100 GeV, and the planned ground-based ACT arrays CTA [58] and AGIS [59]. We demonstrate that, in the case that a gamma-ray signal is clearly detected, the origin could be identified as decay, annihilation, or both by examining the dependence of the intensity and energy spectrum on the angular distribution of the emission. Furthermore, if annihilation and decay each contribute significantly to the signal, we show how these observations could be used to extract information about the dark matter mass, lifetime, annihilation cross section, and dominant annihilation and decay channels. In addition, as a byproduct of this analysis, one might also establish or limit the contribution to the signal from substructure in the dwarf galaxy's halo.

The paper is organized as follows. We outline our proposed observing strategy in §2. In §3 we summarize the properties of the dwarf galaxies we consider and describe our approach to modeling their dark matter halos and subhalos. The gamma-ray spectra from dark matter annihilation and decay are discussed in §4. In §5 we demonstrate the proposed method by presenting example results for various dark matter scenarios for selected dwarf galaxies. We summarize our results and conclude in §6.

2. Method

An indirect signal from annihilation or decay originates from the same dark matter particles, but these two processes give rise to different angular distributions of the emission and different energy spectra. We propose an observing strategy to distinguish these two processes by the angular variation of the intensity and the energy spectrum of the signal. We first describe the general case of gamma-ray observations of an external halo (specifically, we assume that the distance from our position to the object is large compared to the size of the region in the object from which the signal originates), and then illustrate the technique for specific dwarf galaxies.

As pointed out in Refs. [60, 61], angular information is crucial to distinguish dark matter annihilation from decay. The rate of annihilation scales as the square of the dark matter density ρ , while that of decay scales linearly with the density, and consequently the angular distribution of the signal from dark matter annihilation in an external halo is expected to follow a steeper profile than that from dark matter decay. However the spatial distribution of dark matter substructure in a halo also scales roughly as ρ in the outer regions of the halo. Consequently, annihilation in this component could produce a similar flattening in the angular distribution of the observed emission as is expected for decay (see, e.g., Fig. 1, discussed in §3).

From an observational standpoint, a dramatic decrease in the observed intensity between the center of the object and that at larger angles is a clear indicator of the simple case of annihilation in the smooth halo only, while the observation of a shallow emission profile at all angles would strongly suggest decay only. On the other hand, the observation of a bright central region but with the intensity falling off more slowly in the outer regions is less straightforward to interpret, as it could indicate annihilation with an important contribution from substructure, or both annihilation and decay contributing significantly. In this case, we demonstrate that an analysis of the energy spectrum of the signal as a function of angular distance from the center of the object could provide the necessary information to distinguish these possibilities.

If only one process (annihilation or decay) produces a detectable signal, the energy spectrum of the dark matter signal is the same from all regions of the object, with the intensity varying according to how the rate of that process depends on the dark matter distribution. If both processes produce detectable signals, the energy spectrum of the total signal varies according to the contribution from each process. With generality, we can assume that in this two-process scenario the annihilation signal is always dominant in the inner regions of the object, with decay becoming more important at larger angles from the center of the object. Thus, we identify that both annihilation and decay are present by observing a change in the energy spectrum of the signal as a function of angle. In the following we further examine the information available from an indirect measurement in the two-process case.

The differential intensity of the gamma-ray signal (photons per time per area per solid angle per energy) at an angle ψ from the center of the object from dark matter

decay or annihilation can be written as the product of a term depending on the particle properties P and a term depending on the dark matter distribution Φ ,

$$I_x(\psi) = P_x \times \Phi_x(\psi) \quad (1)$$

where $x = \text{D}$ or A , for decay and annihilation, respectively. The particle physics factors are defined as

$$P_{\text{D}} = \frac{1}{m_\chi \tau_\chi} \frac{dN_{\text{D}}}{dE} \quad (2)$$

$$P_{\text{A}} = \frac{\langle \sigma v \rangle}{2m_\chi^2} \frac{dN_{\text{A}}}{dE} \quad (3)$$

where m_χ is the mass of the particle, τ_χ is the lifetime, $\langle \sigma v \rangle$ is the annihilation cross section, and dN_{D}/dE and dN_{A}/dE are the differential photon spectra per decay or annihilation, respectively. The $\Phi_x(\psi)$ are determined by the dark matter density profile which can be estimated from kinematic data, and the dN_x/dE are set by the channels for each process. However, we emphasize that in general this is insufficient information to determine the particle physics properties, since for a given final state, the mass of the dark matter particle that produces the observed gamma-ray spectrum is a factor of 2 larger in the case of decay than in annihilation. The angular dependence of the spectral information is essential to distinguish the two processes and break the degeneracy.

Since there are parameters that determine the intensity from annihilation and decay that are common to both processes, we can distill the information contained in the indirect signal by considering the ratio of the intensity at a given ψ from annihilation to decay,

$$\frac{I_{\text{D}}(\psi)}{I_{\text{A}}(\psi)} = \frac{P_{\text{D}}}{P_{\text{A}}} \frac{\Phi_{\text{D}}(\psi)}{\Phi_{\text{A}}(\psi)} = \frac{2m_\chi}{\langle \sigma v \rangle \tau_\chi} \frac{(dN_{\text{D}}/dE)}{(dN_{\text{A}}/dE)} \frac{\Phi_{\text{D}}(\psi)}{\Phi_{\text{A}}(\psi)}. \quad (4)$$

For a specified density profile and set of annihilation and decay channels the ratio of the intensities of the two signals at a given angle depends only on the particle properties. Defining the angle at which the two signals are equal at a given energy (or, in practice, integrated over some energy range) as ψ_{cross} , we can write

$$\tau_\chi = \frac{2m_\chi}{\langle \sigma v \rangle} \frac{\int dE (dN_{\text{D}}/dE) \Phi_{\text{D}}(\psi_{\text{cross}})}{\int dE (dN_{\text{A}}/dE) \Phi_{\text{A}}(\psi_{\text{cross}})}. \quad (5)$$

A measurement of ψ_{cross} thus determines the value of the lifetime in terms of the mass and annihilation cross section. However, a key point in this scenario is that by measuring ψ_{cross} , the presence of both annihilation and decay is confirmed, so by examination of the signal in the inner and outer regions of the object, the degeneracy in the dark matter particle mass m_χ could be broken. In this case the particle properties τ_χ and $\langle \sigma v \rangle$ are also uniquely determined from the indirect measurement, up to uncertainties in the density profile and, for the signal from the outer regions, uncertainties in the properties of substructure. These uncertainties in the dark matter distribution enter into $\Phi_{\text{A}}(\psi_{\text{cross}})$ and $\Phi_{\text{D}}(\psi_{\text{cross}})$.

In the following sections we discuss in detail the approach outlined here for the case of gamma-ray observations of dwarf galaxies. We illustrate the proposed method

for selected dwarfs, show the expected signals for several example benchmark dark matter scenarios, and indicate the range of dark matter particle parameters for which a transition between annihilation and decay would occur in these objects.

3. Dwarf galaxies

Dwarf galaxies are extremely dark-matter-dominated, with mass-to-light ratios in the range $100 M_{\odot}/L_{\odot} < M/L < 1000 M_{\odot}/L_{\odot}$ [62, 63]. High dark matter densities coupled with minimal foregrounds due to a scarcity of astrophysical gamma-ray sources make these objects excellent targets for indirect dark matter searches in GeV and TeV gamma-rays [34, 40–48]. The predicted emission from dark matter decay or annihilation in Milky Way dwarfs has a large angular extent (\sim few degrees), which makes it possible to map the angular distribution of an observed signal.

We illustrate the proposed technique for three Milky Way dwarf galaxies: Draco, Ursa Minor, and Sagittarius. These dwarf galaxies are among the most optimistic for detection in gamma-rays (e.g., Refs. [43, 48]), and are all accessible targets for dark matter searches with HESS, VERITAS, or MAGIC. It is important to note that Sagittarius is undergoing tidal disruption by the Milky Way which induces substantial uncertainties in the structural properties of this dwarf galaxy, and in turn in the predicted annihilation and decay signals. However, due to its close proximity and inferred large mass-to-light ratio Sagittarius is often considered an excellent target for dark matter searches in gamma-rays, so for this reason we include it here.

The dominant gamma-ray signal from dark matter annihilation or decay in dwarf galaxies of the Milky Way is produced in conjunction with the hadronization, fragmentation, and subsequent decay of the Standard Model particles in the final states. In channels with charged leptons in the final states, internal bremsstrahlung gamma-rays are also generated. In addition, energetic electrons and positrons produced in these processes give rise to secondary photons at various wavelengths via inverse Compton scattering off the ambient photon background and synchrotron emission due to the presence of magnetic fields. Since both the magnetic field and starlight density in dwarf galaxies are small, the dominant energy loss mechanism for electrons and positrons at GeV–TeV energies is expected to come from the upscattering of Cosmic Microwave Background photons, resulting in secondary photons with significantly smaller energies than the primary gamma-ray emission from these channels [64–67]. Thus, this secondary emission is only significant at the lowest part of the energy ranges considered here and only for some channels, so for simplicity we ignore this contribution.

Substructure in the halo of a Milky Way-sized galaxy, including multiple generations of nested sub-subhalos, is resolved in numerical simulations, including subhalos with properties matching those of known dwarf galaxies [68–70]. Simulations indicate that the dark matter density profiles of dwarf-galaxy-sized satellites can be described by the canonical density profiles used to describe larger halos, although some uncertainties remain since tidal disruption may lead to mass redistribution, e.g., significant mass loss

in the outer regions of the halo [71–74]. The properties of substructure in dwarf galaxy halos are even less certain, but for completeness we consider this possibility as well.

The dwarf’s halo and its subhalos were likely formed before tidal stripping of the dwarf halo took place. Since studies suggest that most of the tidal mass-loss occurs in the outer regions of the halo, leaving the inner regions largely intact, we set the properties of the halos and subhalos before any tidal effects, and only account for tidal effects by truncating the dwarf halo at a radius r_{cut} (c.f. §3.1) when performing the line-of-sight integral for the intensity calculations. In essence, we assume that all of the mass, smooth and subhalos, outside of r_{cut} has been removed by tidal stripping, while everything within r_{cut} remains unchanged.

We treat separately the contributions from the smooth halo and substructure components to the gamma-ray signal. The smooth halo case alone provides a lower limit on the gamma-ray signal from annihilation for our assumed density profile and represents the steepest angular emission profile. On the other hand, simulations indicate that a scaled-down host subhalo population represents the maximum expected abundance of sub-substructure [68, 69], so we model the subhalo population of each dwarf in this way to consider the upper limits on the total annihilation flux and on the shallowness of the angular emission profile in the annihilation case.

3.1. The smooth halo

We describe the mass distribution of the smooth dark matter halo of each dwarf galaxy by a Navarro, Frenk and White (NFW) density profile [75]

$$\rho_{\text{sm}}(r) = \frac{\rho_s}{r/r_s (1 + r/r_s)^2}, \quad (6)$$

where r is the distance to the center of the object, ρ_s is a characteristic density, and r_s is a scale radius. To account for tidal stripping of the outer regions of the dwarf’s halo we truncate the profile at a radius r_{cut} given by the Roche-limit criterion

$$r_{\text{cut}} \simeq \left(\frac{GM_{\text{dwarf}} d_{\text{GC}}^2}{2\sigma_{\text{MW}}^2} \right)^{1/3}, \quad (7)$$

where M_{dwarf} is the mass of the dwarf’s halo used here to determine the tidal radius, d_{GC} is its distance to the Galactic Center, and σ_{MW} is the velocity dispersion of the Milky Way at the satellite’s position. Following Ref. [76], we conservatively adopt $M_{\text{dwarf}} = 10^9 M_{\odot}$, rather than the virial mass M_{halo} implied by each dwarf’s structural parameters (c.f. §3.2), and $\sigma_{\text{MW}} = 200$ km/s to determine the tidal radius of each dwarf’s halo. However, the virial halo mass M_{halo} , not M_{dwarf} , is used in the following sections to set the structural properties of each dwarf halo and its subhalo population. Measured and derived properties of the dwarf galaxies considered here are summarized in Table 1.

Now, writing explicitly the factor Φ in Eq. 1, the intensity I_{sm} from dark matter annihilation or decay in the smooth halo from an angle ψ between the line-of-sight direction and the center of the object is

$$I_{\text{sm},x}(\psi) = \frac{P_x}{4\pi} \int_{l_{\text{os}}} ds \rho_{\text{sm}}^i(r(s, \psi)). \quad (8)$$

Table 1. Measured and derived properties of selected dwarf galaxies. Heliocentric distance d_{\odot} is taken to be the distance to the center of the object. The values of r_s and v_{\max} are taken from Ref. [74], and following Ref. [41], we adopt the same values for these parameters for Sagittarius as for Draco. The scale density ρ_s is derived from r_s and v_{\max} assuming a NFW density profile, and the tidal radius r_{cut} is calculated from Eq. 7. See text for details.

Object	d_{\odot} (kpc)	d_{GC} (kpc)	r_s (kpc)	v_{\max} (km/s)	ρ_s ($M_{\odot} \text{ kpc}^{-3}$)	r_{cut} (kpc)	Refs.
Draco	76	76	0.795	22	6.6×10^7	6.8	[77, 78]
Ursa Minor (UMi)	66	68	0.795	21	6.0×10^7	6.3	[78]
Sagittarius (Sgr)	24	16	0.795	22	6.6×10^7	2.4	[78]

For decay $(i, x) = (1, \text{D})$ and for annihilation $(i, x) = (2, \text{A})$. For observations of the inner regions of Milky Way dwarf galaxies we take $\psi = R/d_{\text{GC}}$ since $R \ll d_{\text{GC}}$, where R is the projected radius from the center of the dwarf. The line-of-sight integral extends from $s = -z_{\max}$ to $s = +z_{\max}$ where $z_{\max} = \sqrt{r_{\max}^2 - R^2}$, and here we take $r_{\max} = r_{\text{cut}}$, given by Eq. 7. The dark matter particle properties are encoded in the factors P_{D} and P_{A} as defined in Eq. 2.

3.2. Substructure

We consider collectively the emission from subhalos within the dwarf galaxy halo, summing over the contribution to the gamma-ray signal from subhalos of all masses. We assume that the density profile of each subhalo can be described by a NFW profile. The individual subhalo differential luminosity L (photons per time per energy) as a function of subhalo mass M_{sub} is proportional to the integral over the subhalo volume of ρ in the case of decay or ρ^2 in the case of annihilation:

$$L_{\text{D}} = P_{\text{D}} \int dV_{\text{sub}} \rho_{\text{sub}} \propto M_{\text{sub}} \quad (9)$$

$$L_{\text{A}} = P_{\text{A}} \int dV_{\text{sub}} \rho_{\text{sub}}^2 \propto M_{\text{sub}} \frac{c^3}{f^2(c)}. \quad (10)$$

The subhalo concentration $c = r_{\text{vir}}/r_s$ where r_{vir} is the virial radius of the subhalo, corresponding to an average enclosed overdensity of 200 times the critical density, and $f(c) = \ln(1+c) + (c/(1+c))$.

We adopt a power-law mass function for the subhalos, $dN/dM \propto M^{-\alpha}$ with $\alpha = 1.9$ and minimum and maximum subhalo mass $M_{\text{min}} = 10^{-6} M_{\odot}$ and $M_{\text{max}} = M_{\text{halo}}$, where M_{halo} is the virial mass of the dwarf halo determined by the density profile parameters given in Table 1, without tidal stripping, within a virial radius r_{vir} .

We note that although subhalo masses are described by the quantity M_{sub} for the purpose of defining a mass-concentration relation, in numerical simulations subhalos are typically identified by measuring the parameters v_{\max} , the maximum circular velocity of particles in the subhalo, and $r_{v_{\max}}$, the radius at which that maximum occurs. These

two parameters are sufficient to specify a NFW density profile for the subhalo and thereby fix the structural properties. The quantity M_{sub} is the mass within the virial radius of a subhalo with a given NFW density profile, with the virial radius as defined previously. It is important to keep in mind that subhalos may suffer mass loss as a result of tidal stripping, and thus M_{sub} may not accurately reflect the current bound mass of the subhalo. As in prior work (e.g., Ref. [39]) based on the results of simulations, M_{sub} is used here in conjunction with the concentration parameter c to parameterize the density profile of the subhalos and determine a L_A - M_{sub} relation. Although the possible impact of tidal stripping, in particular the corresponding decrease of the bound subhalo mass, on the annihilation luminosity is expected to be small since most annihilation occurs in the inner regions of the subhalo, the effect on the decay luminosity could be greater. However, as the decay signal from substructure is subdominant with respect to the smooth halo decay signal at all radii we consider (see Fig. 1), we do not attempt to account for this uncertain effect here.

The mass-luminosity relation for annihilation can be approximated by $L_A \propto M_{\text{sub}}^\beta$ with $\beta = 0.87$ (0.94) for M_{sub} greater than (less than) $10^6 M_\odot$. The value of β is determined from Eq. 10 using the subhalo mass-concentration relation from Ref. [39], i.e., $c_{\text{sub}}(M_{\text{sub}}) \propto M_{\text{sub}}^\delta$ with $\delta = -0.06$ (-0.025) for M greater than (less than) $10^6 M_\odot$.

The particle physics factor can be separated from the contribution to the luminosity depending on the subhalo density profile by defining $\mathcal{L}_x = L_x/P_x$, and hence we can write

$$\frac{dN}{d\mathcal{L}} = \frac{dN}{dM} \frac{dM}{d\mathcal{L}}. \quad (11)$$

The mass function is normalized such that $\int_{M_{\text{min}}}^{M_{\text{max}}} dN/dM = 1$, so integrating the individual subhalo \mathcal{L}_x over the mass function gives the average contribution to the decay or annihilation rate from a single subhalo

$$\mathcal{L}_{\text{subs,D}} = \frac{f_{\text{subs}} M_{\text{halo}}}{N_{\text{subs}}} \quad (12)$$

$$\mathcal{L}_{\text{subs,A}} = \int_{\mathcal{L}_{\text{min,A}}}^{\mathcal{L}_{\text{max,A}}} d\mathcal{L}_A \mathcal{L}_A \frac{dN}{d\mathcal{L}_A} \quad (13)$$

where f_{subs} is the mass fraction in substructure and $\mathcal{L}_{\text{min,A}}$ and $\mathcal{L}_{\text{max,A}}$ are the values of \mathcal{L}_A corresponding to M_{min} and M_{max} , respectively.

The intensity in a direction ψ from subhalos, analogous to the smooth halo intensity given in Eq. 8, is then given by

$$I_{\text{subs},x}(\psi) = \frac{P_x}{4\pi} \int_{l_{\text{os}}} ds \mathcal{L}_{\text{subs},x} n_{\text{subs}}(r(s, \psi)), \quad (14)$$

where $n_{\text{subs}}(r)$ is the number density of subhalos at a radius r from the halo center.

Following the results of recent numerical simulations we describe the radial distribution of subhalos with an Einasto profile [79]:

$$n_{\text{subs}}(r) \propto \exp \left\{ -\frac{2}{\alpha_{\text{Ein}}} \left[\left(\frac{r}{r-2} \right)^{\alpha_{\text{Ein}}} - 1 \right] \right\}, \quad (15)$$

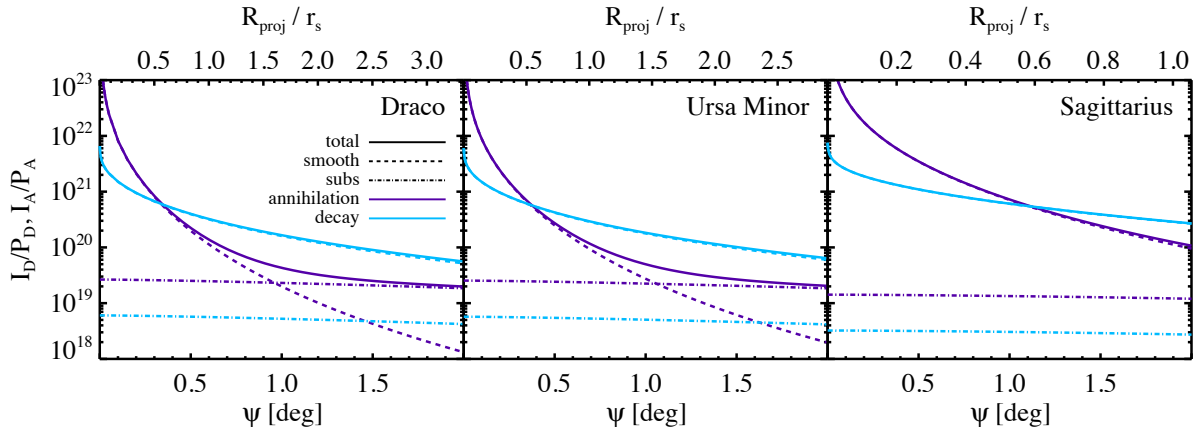


Figure 1. Dependence of the intensity from decay (*blue*) and annihilation (*purple*) on line-of-sight direction ψ from the center of the object for selected dwarf galaxies. The contributions from the smooth halo (*dashed*), substructure (*dot-dashed*), and the total (*solid*) are shown. The corresponding projected radius R_{proj} in units of the halo scale radius r_s is labeled on the top axis. For generality, the amplitudes of the curves for decay and annihilation have been scaled by the factors P_D and P_A respectively, which depend on the assumed particle properties. I_D/P_D is shown in units of $\text{GeV cm}^{-2} \text{sr}^{-1}$, and I_A/P_A is shown in units of $\text{GeV}^2 \text{cm}^{-5} \text{sr}^{-1}$.

with $\alpha_{\text{Ein}} = 0.68$ and $r_{-2} = 0.81 r_{\text{vir}}$, as in Ref. [69]. The subhalo number density is normalized so that 10% of the mass of the smooth halo is condensed into subhalos with masses between 10^{-5} and $10^{-2} M_{\text{halo}}$. For the dwarf galaxies considered here, this results in $\sim 30\%$ of M_{halo} bound in substructure.

The angular dependence of the gamma-ray intensity from annihilation and decay is shown in Fig. 1 for our three example dwarf galaxies. The contributions from substructure and the smooth halo are shown separately, along with the total of these signals from each process. Note that we have not subtracted the subhalo mass density from the smooth halo in determining the signals from annihilation and decay in the smooth halo, so for scenarios with substructure, this leads to a slight overestimate of the smooth halo signal and correspondingly, the total signal. This is a negligible effect for annihilation since the correction to the mass density applies preferentially to the outer regions of the halo where the subhalos represent a larger mass fraction, and where the smooth halo annihilation signal is small and subdominant to the substructure annihilation signal. Likewise, this correction is a small effect for decay, so for simplicity we do not account for it here. The contribution from annihilation or decay in substructure (blue and purple dot-dashed curves) tends to be nearly parallel to the smooth halo contribution in the case of decay (blue dashed curves) at angles $\gtrsim 1^\circ$. This is expected, as the number density of subhalos scales approximately as ρ_{sm} outside of the inner region of the halo, as the dark matter decay rate in the smooth halo does. Note that decay in substructure is always subdominant relative to decay in the smooth halo, even in the maximal substructure scenario we consider here. The shapes of the curves are quite similar for all three objects, however the amplitude of the curves

for Sagittarius is somewhat larger, reflecting the fact that this dwarf galaxy has similar structural properties to the other two but is at a significantly smaller distance.

4. Gamma-ray spectra from dark matter annihilation and decay

With the goal of presenting the results in a general and model-independent way, we consider here the generic features in the gamma-ray spectrum implied by dark matter annihilations and decays, whose products we will assume to be two Standard Model particles. Cases with additional SM particles in the final state and more exotic scenarios have also been considered [80–82]. An investigation of the use of our proposed method in those cases would require additional dedicated analyses.

The spin of the state constituted by the s-wave of two non-relativistic dark matter particles can only have integer values (if it is a WIMP, it can only be 0, 1 or 2). Thus, annihilation of dark matter particles with mass m_χ can be described as the decay of the s-wave of a state with mass $2m_\chi$ and integer spin [18]. Hence, the possible final states (at tree level) with only two Standard Model particles produced from dark matter annihilations are: W^+W^- , ZZ , Zh , hh , l^+l^- and $q\bar{q}$, where l and q represent any lepton or quark, respectively.

On the other hand, the allowed channels from dark matter decay are much less constrained and, in principle, the spin of the initial state can be integer or half-integer. Although mixed channels involving a Standard Model particle and a new particle or three-body decays are possible, we will not consider these possibilities and instead restrict our study to the case of only two Standard Model particles in the final state. In the case of decays, in addition to the allowed channels for annihilation, which correspond to scalar dark matter decay, there is the possibility of semileptonic channels, such as W^+l^- , if dark matter is a fermion.

We simulate the hadronization, fragmentation and decay of different final states with the event generator PYTHIA 6.4 [83]. For each mass and channel we consider 10^7 events distributed in 500 logarithmically-spaced energy bins. In Fig. 2 we show the gamma-ray spectra for a 400 GeV dark matter particle for annihilation (upper panels) and decay (lower panels). In the left panels we show the leptonic and semileptonic (decay-only) channels, whereas in the right panel we show the hadronic and gauge boson channels. It is clear from the figure that leptonic channels typically give rise to a harder spectrum. Indeed, in the case of leptonic channels (in particular e^+e^- and $\mu^+\mu^-$), the cutoff would be very sharp around a maximum energy. We emphasize, however, that the presence of this cutoff in the spectrum would not allow one to determine the dark matter mass unless one knows if the signal comes from annihilation or decay, due to the factor of 2 difference in the cutoff energy between these processes.

As it can be seen in the figure, one could generically classify the spectra associated with these final states as either soft (hadronic or gauge boson) or hard (leptonic), with semileptonic channels being a mixture of the two. Thus, for the sake of simplicity when showing explicit examples, we will consider combinations of soft-hard or hard-

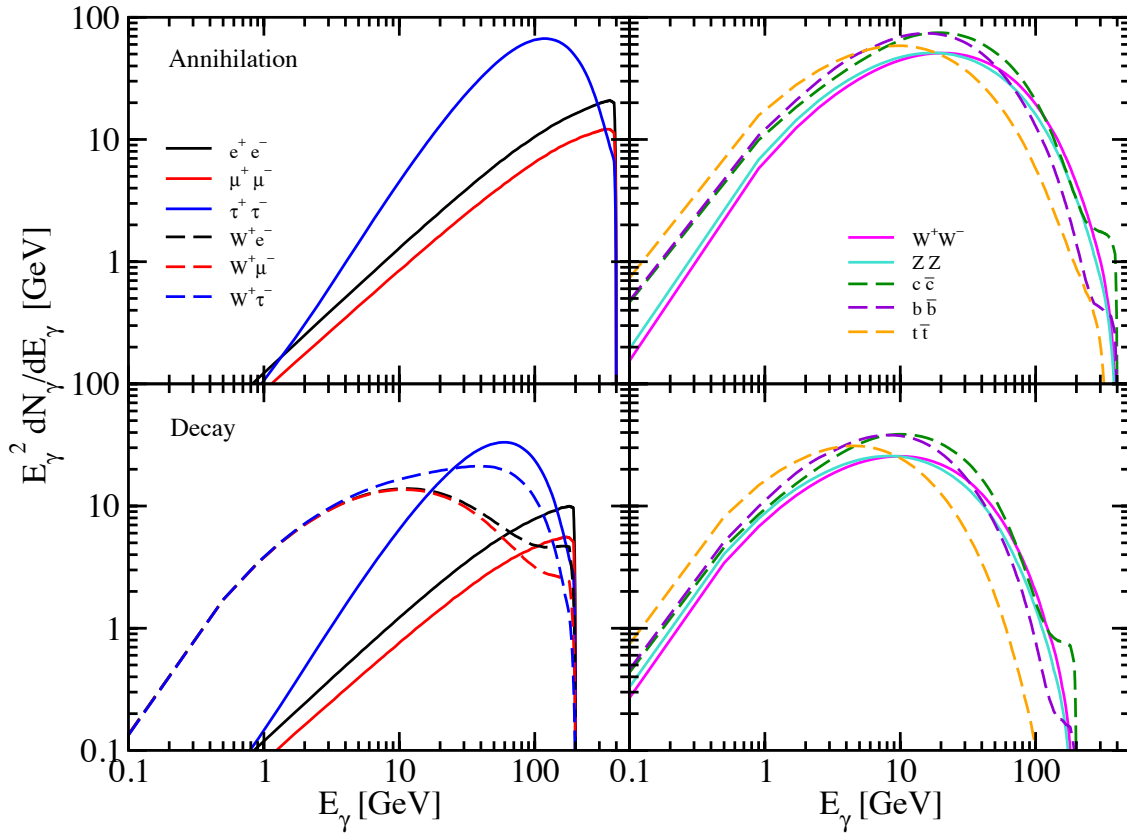


Figure 2. Energy spectra ($E_\gamma^2 dN_\gamma/dE_\gamma$) for different possible final states with two Standard Model particles for a 400 GeV dark matter candidate. In the upper panels we show the case of annihilation and in the lower panels that of decay. *Left panels:* leptonic and semileptonic channels, as labeled. Note that the semileptonic channels (W^+e^- , $W^+\mu^-$, and $W^+\tau^-$) can only be present for decay. *Right panels:* hadronic and gauge boson channels, as labeled.

soft channels for annihilation-decay, which in general represent the extreme cases. We comment that although it is possible for the dominant final states for both annihilation and decay to be the same (which would yield similarly shaped energy spectra), the maximum energy of the photons from dark matter annihilation is twice the energy of those from dark matter decay. Thus, as can be seen from Fig. 2, in general the gamma-ray spectra from dark matter annihilation and decay are different ‡.

‡ In the case of dark matter annihilation dominantly into top quarks and decay dominantly into any of the other hadronic or gauge boson channels shown in Fig. 2, the distinction, on the basis of the energy spectra alone, might be challenging.

5. Results

The aim of this work is to propose an observing strategy to maximize the information that could be obtained from gamma-ray experiments in the case that a signal from dark matter is clearly detected. Our goal is not to evaluate the detectability of specific scenarios with current instruments; for the interested reader we reference some of the many studies that have carefully addressed that subject with observations of dwarf galaxies [44–48]. However, let us emphasize that in order for this approach to be applicable with current experiments, a signal just beyond the limits established so far must be discovered to yield sufficient statistics to map the signal and determine the energy spectrum over an extended angular region.

The first requirement in order to use this technique is that the source is resolved as an extended source. In particular, we assume that the signal can be binned into several annuli centered on the source. This is in principle possible with the angular resolution of current experiments ($\sim 0.1^\circ$ at the relevant energies) for observations of dwarf spheroidal galaxies, since the angular extent of the predicted dark matter signal is as large as \sim few degrees. In addition, this technique requires that the signal in each annulus is detected with sufficient statistics to reconstruct the energy spectrum. In the following we proceed under the assumption that a signal meeting these conditions has been detected.

In Fig. 3 we illustrate the proposed method for a scenario in which both annihilation and decay contribute appreciably to the observed signal from the Draco dwarf galaxy by showing the energy spectrum as a function of the angle from the center of the object. The energy spectrum in alternating annuli of 0.1° width centered on Draco is shown out to an angular radius of 0.9° (from top to bottom) for a dark matter particle mass of $m_\chi = 200$ GeV. Two combinations of channels are shown. The left (right) column shows the case of annihilation into a soft (hard) channel and decay into a hard (soft) one. The channels $\mu^+\mu^-$ and W^+W^- have been chosen as representative of hard and soft channels, respectively. In each panel, dashed lines represent the contribution from decay, dotted lines represent that from annihilation, and the thick solid lines represent the total contribution. We have taken $\langle\sigma v\rangle = 3 \times 10^{-26}$ cm³ s⁻¹ and $\tau_\chi = 10^{29}$ s. Note that although we have included the contribution of substructure, it is a subdominant effect for both annihilation and decay for the annuli considered in this figure (see Fig. 1). The presence of substructure increases the contribution from annihilation primarily in larger annuli than shown in this figure. As expected, a significant change in the spectrum is clearly seen in Fig. 3 for both combinations of channels at around $E = m_\chi/2$, i.e., the maximum energy for photons from dark matter decay. The spectral change is a signature of both annihilation and decay contributing significantly to the signal.

As a summary of the discussion above, in Fig. 4 we show the contributions, again including substructure, from the innermost (black lines, $[0.0^\circ, 0.1^\circ]$) and the outermost (red lines, $[1.9^\circ, 2.0^\circ]$) annuli we consider, for $m_\chi = 200$ GeV. We show the results for the three studied dwarf galaxies for the same two combinations of channels as in Fig. 3,

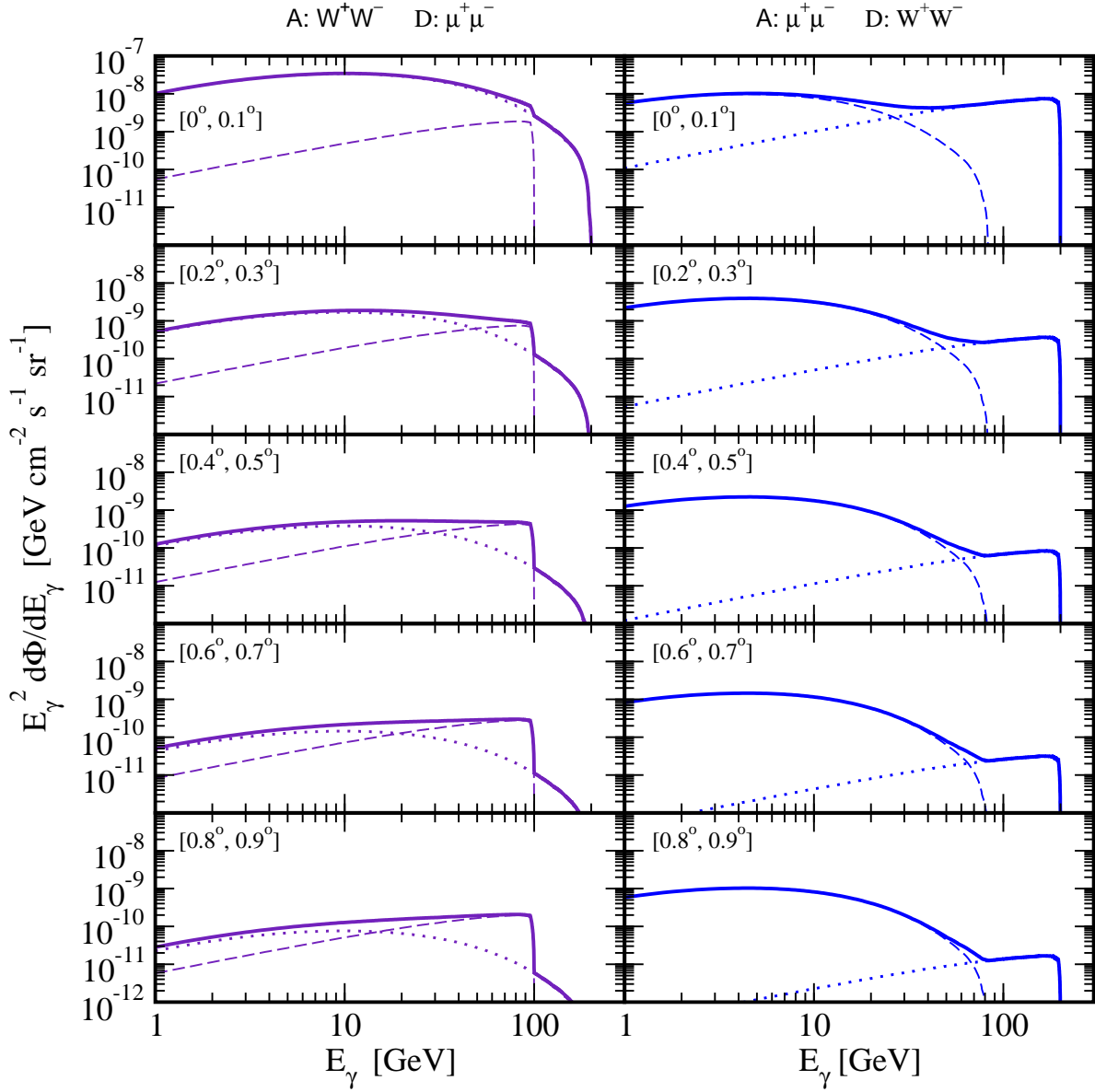


Figure 3. Energy spectra in different annuli centered on Draco for $m_\chi = 200$ GeV and for two combinations of channels. *Left panels:* Annihilation into W^+W^- (soft) and decay into $\mu^+\mu^-$ (hard). *Right panels:* Annihilation into $\mu^+\mu^-$ (hard) and decay into W^+W^- (soft). Dotted lines represent the contribution from annihilation, dashed lines that from decay, and solid lines the sum of the two. In each column, the spectra for alternating annuli of 0.1° width is shown, with the innermost annuli in the top panels. The contribution from substructure is included and here we take $\langle\sigma v\rangle = 3 \times 10^{-26} \text{ cm}^3 \text{ s}^{-1}$ and $\tau_\chi = 10^{29} \text{ s}$. The change in the shape and amplitude of the total (*thick solid lines*) from inner to outer annuli indicates that both annihilation and decay are present.

as indicated, and the same values for the annihilation cross section and lifetime are used as in Fig. 3. The changes in spectral shape and amplitude between the innermost and outermost annuli are easily identified.

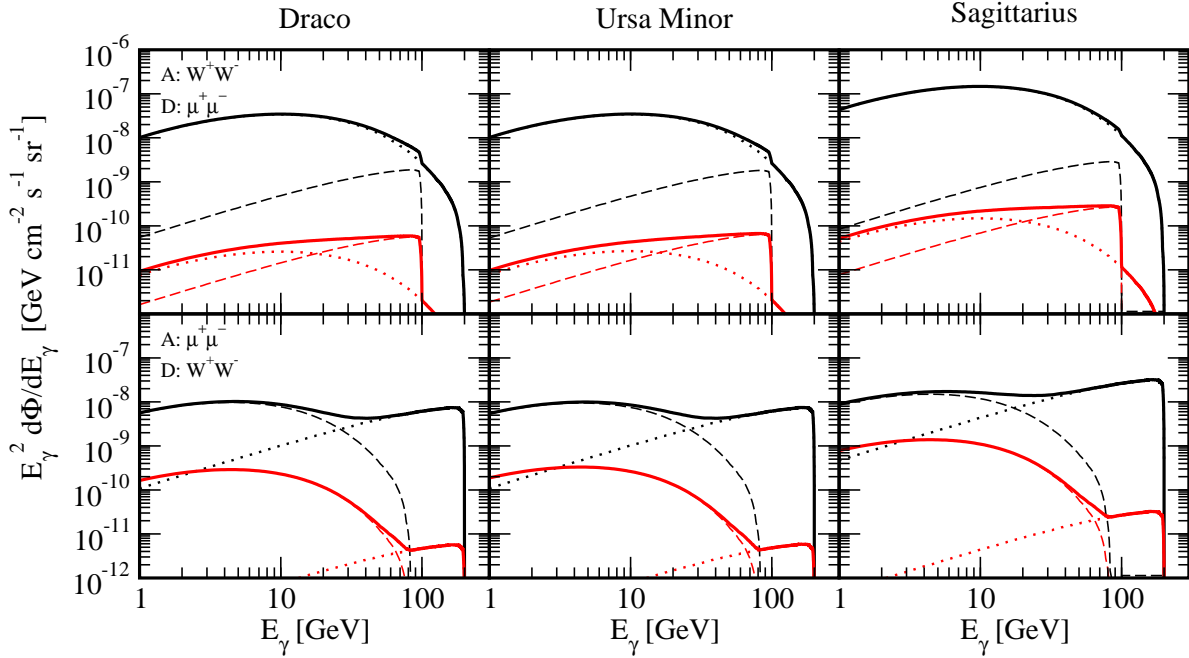


Figure 4. Energy spectra for $m_\chi = 200$ GeV from the contribution of the innermost annuli (*black lines*, $[0.0^\circ, 0.1^\circ]$) and the outermost annuli (*red lines*, $[1.9^\circ, 2.0^\circ]$) we consider, for three dwarf galaxies. We show in the upper and lower panels the same two combinations of channels as in Fig. 3, adopting the same values for $\langle\sigma v\rangle$ and τ_χ and again including substructure. As in Fig. 3, dotted lines indicate the contribution from annihilation, dashed lines that from decay, and the thick solid lines show the total signal.

On the other hand, we also show in Fig. 5 an example for two dark matter models that could potentially explain the PAMELA data: one in terms of decay as the primarily contributor plus a negligible contribution to the PAMELA signal from annihilation with a thermal cross section (solid lines), and one in which decay and annihilation each contribute similarly to the PAMELA signal (dashed lines). We depict the the total contribution for $m_\chi = 200$ GeV from dark matter annihilation plus decay for the three dwarf galaxies and for two channels: $\mu^+\mu^-$ (top row) and $\tau^+\tau^-$ (bottom row). In each row, the same channel is assumed for both annihilation and decay rather than combinations of channels as in Figs. 3 and 4. For the $\mu^+\mu^-$ case, $\tau_\chi = 7 \times 10^{26}$ s and $\langle\sigma v\rangle = 3 \times 10^{-26}$ $\text{cm}^3 \text{s}^{-1}$ for the dominantly-decay scenario (solid lines) while $\langle\sigma v\rangle = 3 \times 10^{-24}$ $\text{cm}^3 \text{s}^{-1}$ for the two-process scenario (dashed lines). For the $\tau^+\tau^-$ case, $\tau_\chi = 2 \times 10^{26}$ s and $\langle\sigma v\rangle = 3 \times 10^{-26}$ $\text{cm}^3 \text{s}^{-1}$ ($\langle\sigma v\rangle = 6 \times 10^{-24}$ $\text{cm}^3 \text{s}^{-1}$) for the solid lines (dashed lines). In each panel, black and red lines represent the result for the innermost ($[0^\circ, 0.1^\circ]$) and outermost ($[1.9^\circ, 2^\circ]$) annulus, respectively. These four cases are found to fit the PAMELA data in the case of decay-only and annihilation-only [81,84], but we have chosen the parameters so that the combination of the two types of signal would also fit the data. We see that very different spectra are obtained from the center of the galaxies as compared to regions further away, which is a clear signature of the presence

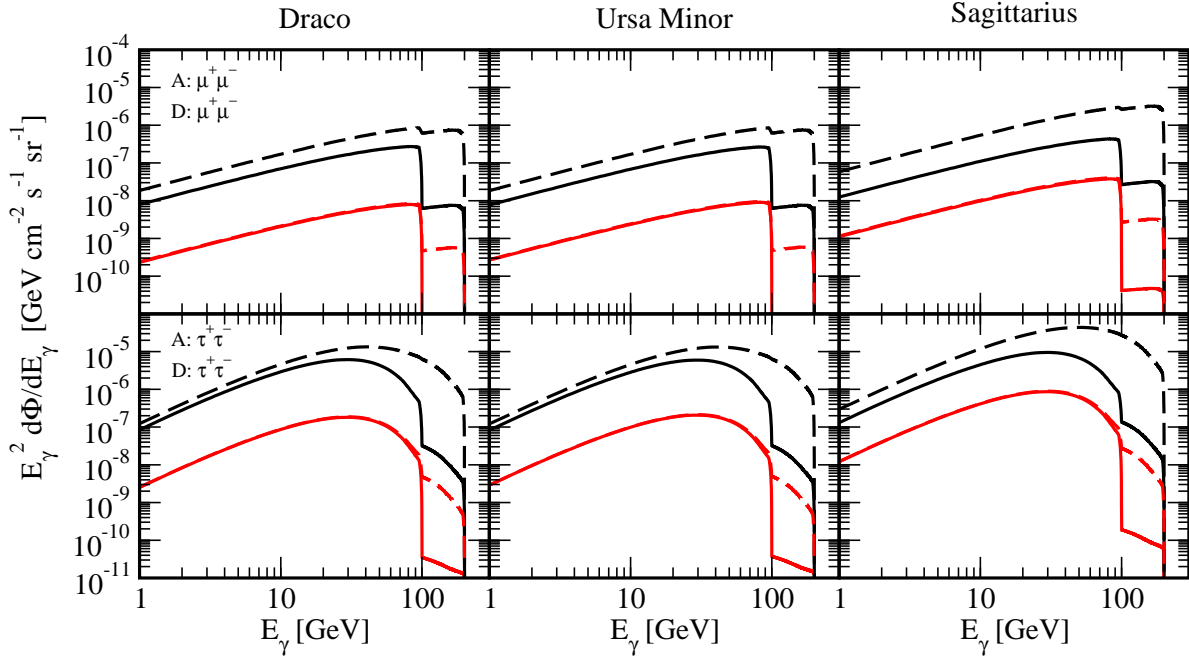


Figure 5. Energy spectra for $m_\chi = 200$ GeV from the contribution of the innermost annuli (*black lines*, $[0.0^\circ, 0.1^\circ]$) and the outermost annuli we consider (*red lines*, $[1.9^\circ, 2.0^\circ]$), for the three studied dwarf galaxies. In each row we assume dark matter annihilates and decays dominantly into the same channel and depict the total contribution. *Upper panels:* $\mu^+\mu^-$, $\tau_\chi = 7 \times 10^{26}$ s and $\langle\sigma v\rangle = 3 \times 10^{-26}$ cm 3 s $^{-1}$ ($\langle\sigma v\rangle = 3 \times 10^{-24}$ cm 3 s $^{-1}$) for the solid (*dashed*) lines. *Lower panels:* $\tau^+\tau^-$, $\tau_\chi = 2 \times 10^{26}$ s and $\langle\sigma v\rangle = 3 \times 10^{-26}$ cm 3 s $^{-1}$ ($\langle\sigma v\rangle = 6 \times 10^{-24}$ cm 3 s $^{-1}$) for the solid (*dashed*) lines. These four cases fit the PAMELA data in decay-only or annihilation-only scenarios [81, 84]. Note that the parameters are chosen so that the total signal would also fit the data.

of dark matter decay as well as annihilation.

Figs. 6 and 7 indicate the range of dark matter parameters which would induce a transition between annihilation and decay in the angular range of 0° - 2° in Draco, (similar results are obtained for the other two dwarf galaxies). Here we neglect the contribution from substructure. The curves indicate the value of the dark matter lifetime at which the intensities from dark matter annihilation and decay integrated above 1 GeV are equal at ψ_{cross} (see Eq. 5, with the integrated photon yield above 1 GeV). The results for dark matter decay into leptonic and semileptonic channels are shown in Fig. 6, and for decay into hadronic and gauge boson channels in Fig. 7. The annihilation channel for each panel is labeled. In these figures we assume a 200 GeV dark matter candidate and an annihilation cross section in terms of $\langle\sigma v\rangle$ typical of thermal dark matter, $\langle\sigma v\rangle = 3 \times 10^{-26}$ cm 3 s $^{-1}$. A larger cross section would displace the curves downwards, scaling τ_χ inversely to the cross section. For a given ψ_{cross} , above the curves annihilation dominates and the emission profile is steeper, while below the curves the dominant contributor is decay and the profile is shallower.

The normalization of the curves depends on the relative photon yields from

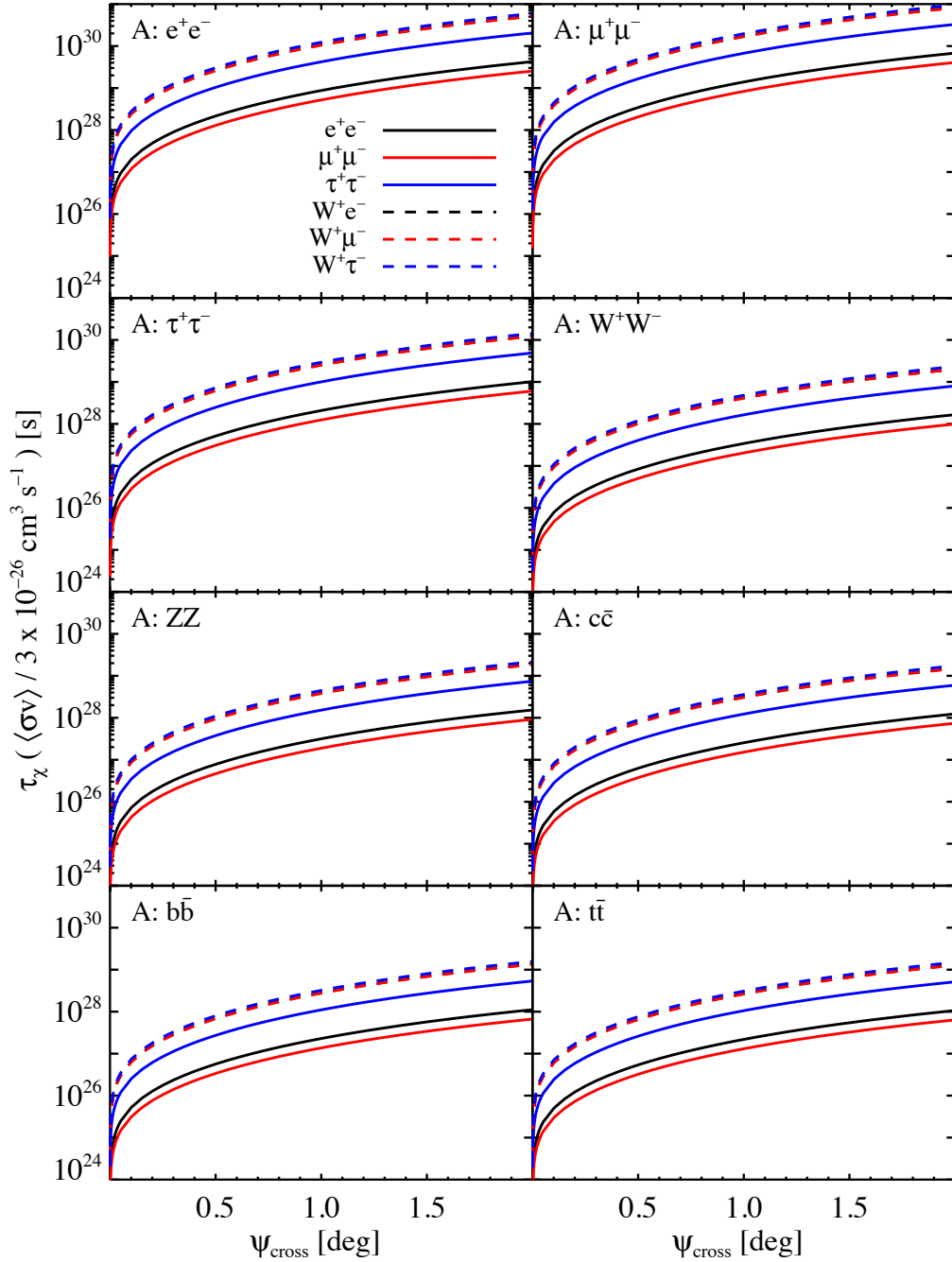


Figure 6. Lifetime τ_χ at which the intensities from annihilation and decay for $E > 1$ GeV are equal at an observation angle ψ_{cross} from the center of the dwarf galaxy, for Draco, without substructure. The dark matter particle mass is $m_\chi = 200$ GeV. Each panel shows curves for a single annihilation channel, assuming decay into leptonic or semileptonic channels (as labeled). The red dashed curves for the $W^+\mu^-$ decay channel fall on top of the black dashed curves for the W^+e^- decay channel because the photon yields above 1 GeV for these two decay channels for this particle mass are almost identical. Smaller values of the lifetime for a fixed annihilation cross-section correspond to smaller values of ψ_{cross} .

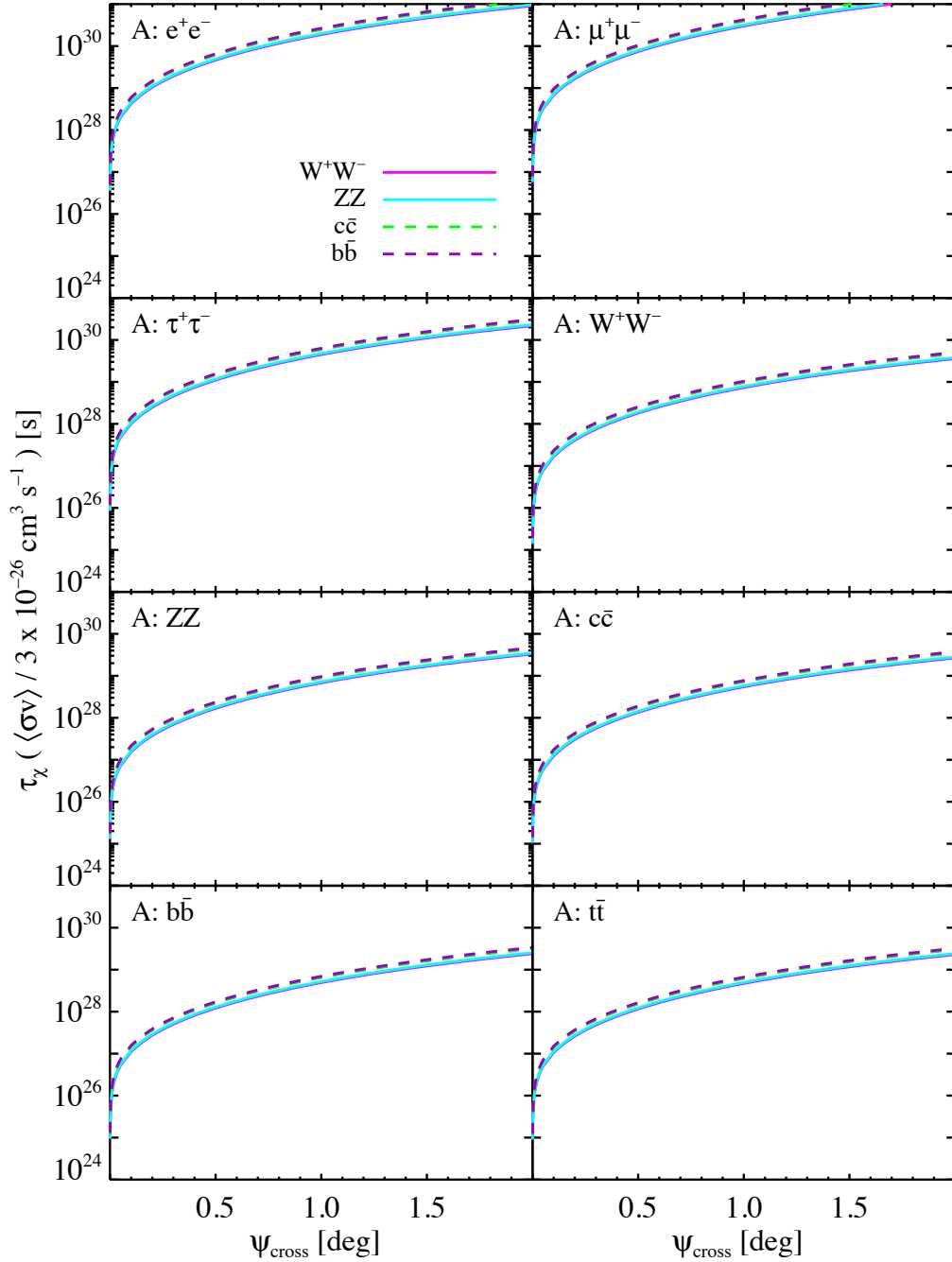


Figure 7. Same as Fig. 6, for hadronic and gauge boson decay channels (as labeled). The four decay channels shown in each panel result in very similar curves due to their similar photon yields above 1 GeV for this particle mass.

annihilation and decay: for a given lifetime, the annihilation-to-decay transition occurs further from the center of the dwarf galaxy for channel combinations in which the ratio of the photon yields from annihilation to decay is larger. In each panel, corresponding to a single annihilation channel, the variation in the amplitude of the curves reflects the different photon yields for the decay channels shown. Decay via any of the hadronic or

gauge boson channels produces almost identical curves since the photon yields above 1 GeV from these channels are similar, and these curves have the highest normalization of any of the channels since their photon yields are the highest. Similarly, there is little difference between the curves for decay into any of the three semi-leptonic channels, and these curves fall below the hadronic and gauge boson decay channel curves. The curves for decay into the leptonic channels show more variation due to the larger variation in photon yields for these channels, and as expected, fall below those for semi-leptonic and hadronic and gauge boson channels due to their relatively low photon yields.

For this energy threshold and an assumed cross section of $\langle\sigma v\rangle = 3 \times 10^{-26} \text{ cm}^3 \text{ s}^{-1}$, in order for the transition to occur at an angle between $\sim 0.1^\circ$ and $\sim 2^\circ$, the dark matter lifetime must be between $\sim 10^{25} \text{ s}$ and 10^{31} s , depending on the combination of channels. Let us note that each individual line in Figs. 6 and 7 extends only over two orders of magnitude. However, this alone does not tell about the sensitivity to the lifetime and annihilation cross section as the range of parameters depend on the particular combination of channels, which is not known. The range of values for the lifetime (for a given annihilation cross section) we mention takes into account our ignorance in this regard. For larger values of the annihilation cross section, correspondingly smaller values of the lifetime are needed.

In Fig. 8, we study the effect of adding substructure and varying the energy threshold of the experiment for two different dark matter masses, $m_\chi = 200 \text{ GeV}$ (left panels) and $m_\chi = 400 \text{ GeV}$ (right panels). We depict two combinations of channels: solid (dashed) lines represent the case of decay into a hard (soft) channel and annihilation into a soft (hard) one. As before, we have chosen $\mu^+\mu^-$ and W^+W^- as representative of hard and soft channels, respectively. In the upper panels we show the results when only the smooth halo contribution is considered and in the lower panels those when substructure is also present. The different colors represent several energy thresholds. For $m_\chi = 200 \text{ GeV}$, we have not considered the threshold of 100 GeV, as this is the maximum energy of the photons from the decay of a dark matter candidate of that mass.

In this figure, the trend explained above regarding photon yields is clearly evident: for the soft-hard combination of channels for annihilation-decay, the transition in the angular emission profile occurs further away from the center than in the hard-soft case. We see that for these masses, there is little difference between using an energy threshold of 0.1 GeV or 1 GeV. However, a higher energy threshold suppresses the contribution of the soft channel and thus the curves are displaced upwards (downwards) if decay is into a hard (soft) channel and annihilation into a soft (hard) one.

In agreement with Fig. 1, Fig. 8 shows that the effect of substructure starts to be important if $\psi_{\text{cross}} \gtrsim 1^\circ$. As it is a very minor correction to the signal from dark matter decay, substructure contributes significantly only to the annihilation signal, and hence it bends the curves in the lower panels downward, indicating that annihilation remains the dominant source of the signal at larger radii. The presence of substructure results in the curves becoming nearly horizontal for $\psi_{\text{cross}} \gtrsim 1^\circ$, i.e., the same ratio of annihilation to

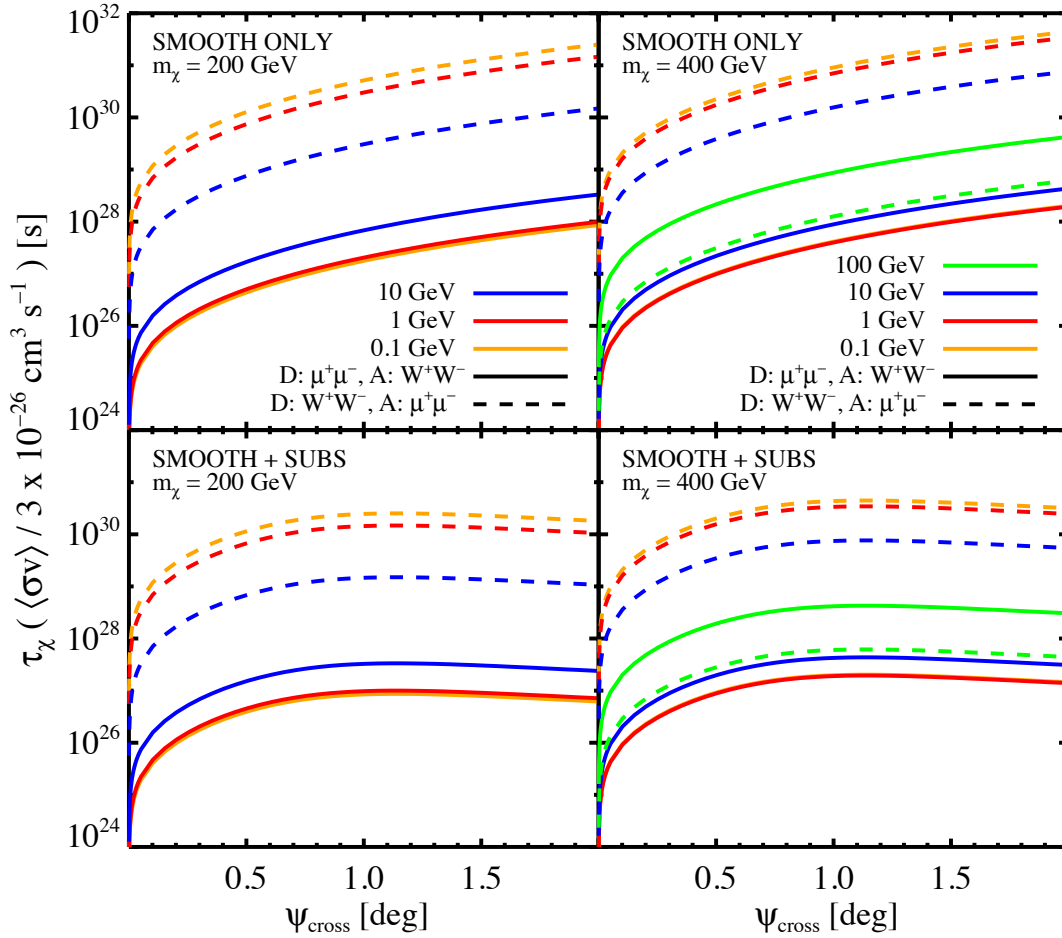


Figure 8. Effect of particle mass, energy threshold, and substructure on the lifetime τ_χ at which the intensities from annihilation and decay are equal at ψ_{cross} from the center of Draco. Each panel shows the results for a hard-soft (*solid curves*) and soft-hard (*dashed curves*) combination of decay-annihilation channels, with $\mu^+\mu^-$ representing a hard channel and W^+W^- a soft channel. In the left panels $m_\chi = 200$ GeV while in the right panels $m_\chi = 400$ GeV. The top panels show the curves for the smooth halo only and the bottom panels include substructure. The results for several choices of energy threshold are shown (as labeled); the curves corresponding to the 100 GeV energy threshold are absent in the left panels since this is the largest possible energy of a photon from the decay of a 200 GeV particle.

decay intensity is maintained at all radii larger than this value. This can be understood by recalling that the substructure contribution to the angular emission profile produces a flattening at large angles very similar to that produced by dark matter decay. Hence, as a first approximation, for $\psi_{\text{cross}} \gtrsim 1^\circ$, there is a limiting value of the lifetime above which decay is always subdominant in the intensity. If the dark matter lifetime is close to that value, the contribution from dark matter decay and annihilation are comparable for $\psi_{\text{cross}} \gtrsim 1^\circ$.

Since the required lifetime to produce a transition at a given angle scales inversely with the annihilation cross section, these figures indicate the ranges of the annihilation

cross section and lifetime for which the transition in the dominant component of the intensity from annihilation to decay occurs within $\sim 0.1^\circ - 2^\circ$ of the center of the dwarf galaxy. Interestingly, current constraints from gamma-ray observations on the decay lifetime place a lower limit of $\sim 10^{25} - 10^{26}$ s depending on the assumed mass and channel [43,82,84–86] (for earlier radiative bounds on the dark matter lifetime in different mass regimes see Refs. [87] and for model-independent bounds see Refs. [61,88]), a range which overlaps slightly with the lower end of the range that would produce a transition within $\sim 1^\circ$ of the center for the dwarfs considered here for a thermal annihilation cross section. Radiative bounds generally constrain the annihilation cross section to be smaller than a factor of $10 - 10^4$ times a thermal cross section, again depending on the mass and channel [48, 82, 84, 89] (see Refs. [90, 91] for other bounds obtained using different techniques). The parameters explored in the examples presented here are therefore broadly representative of scenarios allowed by current data and, moreover, include regions of parameter space that may become accessible in the near future.

6. Discussion and Conclusions

In this work we have outlined a strategy to constrain dark matter properties in the event of the clear detection of an indirect signal from gamma-ray observations of dwarf galaxies. We addressed the question of how scenarios of dark matter annihilation, decay, or both could be distinguished, and what information could be obtained about the intrinsic properties of the dark matter particle and its small-scale distribution from this type of indirect measurement.

In principle, the indirect detection of dark matter in gamma-ray experiments would provide the energy spectrum of the signal. The spectrum from dark matter annihilation has a maximum energy equal to the dark matter particle mass, while the spectrum from decay has a cutoff at half the mass. Consequently, spectral information alone is insufficient to identify the process that produced the signal. However, in addition to the difference in the endpoint of the energy spectrum, annihilation and decay give rise to different angular distributions of the intensity of the emission. Using this information, we demonstrated that if a dark matter signal is clearly detected from a dwarf galaxy, an analysis of the energy spectrum of the emission as a function of the angular distance from the center of the object could provide the necessary information to distinguish the cases of annihilation, decay, or both.

The technique we propose, which combines spectral and angular information, is particularly important due to the uncertainties in the presence and properties of substructure in a dwarf galaxy halo. In particular, whereas the annihilation rate scales as the square of the dark matter density, the decay rate depends linearly on the density. However, the angular distribution of the annihilation (or decay) signal from dark matter substructure also scales approximately linearly with the smooth halo density in the outer regions of the object, so its angular distribution roughly mimics that from dark matter decay in the smooth halo. Furthermore, since the amplitude

of the signal from annihilation in substructure depends sensitively on the properties of the subhalo population and is not fixed by the smooth halo density profile, the relative amplitude of the annihilation signals from substructure and the smooth halo is effectively independent (e.g., Ref. [39]). Thus, identifying annihilation in the smooth halo based on the emission profile in the central regions of the object is not sufficient to distinguish between annihilation in substructure or decay as the origin of emission from the outer regions of the halo.

In order to break this degeneracy, we have studied the energy spectrum as a function of the angular distance from the center of the object (see Figs. 3 and 4). If a flattening in the radial distribution of the intensity of the signal is observed at an angular distance ψ_{cross} (c.f. Eq. 5), this would point either to a significant contribution from both dark matter annihilation and decay or to only dark matter annihilation with an important contribution from substructure. We have shown that a change in the energy spectrum along with the change of slope in the angular distribution could provide the necessary information to confirm or reject the presence of a signal from dark matter decay.

If dark matter decay is established by an observed spectral change as a function of angle, the signal in the innermost parts could be studied to provide information about the annihilation contribution, and that in the outermost regions (beyond ψ_{cross}) would provide information about the decay signal. In principle, determining ψ_{cross} and the intensity of the signal in the inner (annihilation-dominated) and outer (decay-dominated) regions, could help to constrain $\langle\sigma v\rangle$, τ_χ and m_χ . In this case, limits on the properties of substructure could also be placed.

On the other hand, if beyond ψ_{cross} the energy spectrum does not change, we expect annihilation in substructure to be the cause of the flattening in the radial distribution and attribute the signal to annihilation. In this case, we could determine to some extent the contribution of substructure and begin to constrain its properties, such as the mass function slope, minimum subhalo mass, and structural properties. The indirect measurement would then yield the particle mass and annihilation cross-section, and the absence of a strong decay signal would enable further limits on decaying dark matter to be placed.

Finally, if decay (annihilation) in the smooth halo can be established as the dominant contribution due to a very shallow (steep) emission profile at all angles, then the mass and lifetime (annihilation cross-section) could be determined, and upper (lower) bounds placed on the annihilation cross-section (lifetime).

In addition, as it is known and we have shown in §4, to a first approximation the annihilation and decay spectra can be classified as soft (due to hadronic or gauge boson channels) or hard (due to leptonic channels). Hence, once the origin of the signal in the different regions is established (annihilation in the smooth halo, annihilation in the smooth halo and substructure, or decay), further information can be obtained about the annihilation and decay channels by studying the energy spectra. On general grounds, in this situation the distinction between dominantly leptonic or dominantly hadronic and gauge boson channels could be achieved.

Our example scenarios focused on the case of a signal from Milky Way dwarf spheroidal galaxies. However we note that, in principle, this method could also be applied to the case of our own galaxy. In that case an appropriate treatment of the secondary photons produced by the prompt electrons and positrons via inverse Compton scattering off the ambient photon background is necessary (see Ref. [92] for a very recent related study). In the case of our galaxy, this contribution is very important (and it could be the dominant one) due to the large light emission by stars and the infrared light as a result of the scattering, absorption and re-emission of absorbed starlight by dust. In addition, in order to recover any information from an observation, the different backgrounds for a potential signal would have to be properly addressed. The galactic center is a complex region, which makes the modeling of these backgrounds a difficult task. All in all, bearing in mind these differences, a similar application of the methodology described here could be possible in the case of the Milky Way.

We have demonstrated the proposed method for different scenarios that could also potentially explain the rise in the positron fraction observed in the PAMELA data [17] (Fig. 5). In the case that these dark matter models produce a detectable gamma-ray signal from dwarf galaxies, we see that if the dark matter interpretation is correct, the observation of the gamma-ray energy spectrum at different angular distances from the center of the dwarf galaxies could help to establish if the origin of the observed positron excess is due to dark matter annihilation, decay, or both.

Finally, in Figs. 6, 7, and 8 we have shown the range of dark matter parameters for which a transition between annihilation and decay would occur within 2° of the center of Draco (similar results are obtained for Ursa Minor and Sagittarius). We have presented the results for different annihilation-decay combinations and see that the dark matter lifetime must be in the range $\sim (10^{25} - 10^{31} \text{ s}) (3 \times 10^{-26} \text{ cm}^3 \text{ s}^{-1} / \langle \sigma v \rangle)$, the actual (narrower) range depending on the combination of annihilation and decay channels. The effect of substructure in the dwarf galaxy halo is shown to be important only for $\psi_{\text{cross}} \gtrsim 1^\circ$. The choice of energy threshold, however, strongly affects the range of τ_χ and $\langle \sigma v \rangle$ probed by this technique (Fig. 8), suggesting that, in the event of a detection, observations covering a large energy range may be able to explore a substantial region of the dark matter annihilation and decay parameter space.

In order to apply the technique proposed in this study, the firm detection of a gamma-ray signal of dark matter origin would be required. Although the main idea of this work is to show the different potential features of a dark matter signal and to describe the method in a detector-independent way, we think it is worthwhile to add a short discussion along these lines.

The main point is to have access to two types of features, those in the angular distribution and those in the energy spectrum. In order to reconstruct the energy spectrum in a given angular bin, a minimum number of photons is necessary. The integrated number of photons in each angular bin scales with the solid angle Ω of the bin, i.e., $\Omega \sim \pi(r_{\text{out}}^2 - r_{\text{in}}^2)$, where r_{out} and r_{in} are the angular radii of the outer and inner edge of each bin. For the equal width annuli used here, Ω increases linearly with

the radius of the bin center, i.e., the annulus centered on 0.85° encompasses 17 times as much solid angle as the annulus centered on 0.05° . Let us assume, for simplicity, that the difference in the total intensity between inner and outer annuli is of the order of 10 to 100 (cf. Fig. 3). The photon flux from within the outer annulus is therefore typically a factor of a few smaller than from the innermost annulus, if the spectral shapes in each annulus are similar. Although the diffuse backgrounds would also scale with solid angle, in the case that the backgrounds are small, sensitivity to a signal a factor of only a few smaller than the signal in the innermost bin would be required to measure the angular dependence of the integrated flux. If the backgrounds are large, sensitivity to signals a factor of 10 to 100 smaller than that in the innermost bin would be necessary.

While the spectra of the inner and outer annuli depend on the specific combination of channels, very roughly we can say the energy spectrum goes as E^{-2} over most of the relevant energy range (see, e.g., Fig. 3), and hence the integrated photon yield over some range scales approximately as E^{-1} . The examples shown in this study use the energy spectrum over 1 to 2 decades in energy, so for equal logarithmic bins in energy, the flux at high energies is $\sim 1 - 10\%$ of the flux at low energies. To reconstruct the energy spectrum, one could require, e.g., a few signal photons in the highest energy bin of the outermost annulus. This optimistically implies that $\mathcal{O}(1000)$ total photons (angle- and energy-integrated) within a 1 degree radius of the source are needed. On general grounds, to get angular information a factor of a few more statistics is necessary than are needed to detect the dark matter signal clearly (i.e., with spectral info) in the first place. Thus, if a signal in current experiments were detected just beyond the current limits, in the future they might have the ability to do a study of this kind, as the signal will improve with exposure. While this coarse estimate does not include a proper treatment of backgrounds, which depend strongly on energy and on the experiment under consideration, we note that the expected value of the photon counts measured by *Fermi* due to the Galactic diffuse gamma-ray background above 1 GeV in a region of 1 degree around the center of the dwarfs considered here after five years is $\sim 100 - 1000$.

In summary, we have shown that a dark matter particle with an annihilation cross-section and lifetime just beyond the limits currently established could produce a clear spectral change on an angular scale within the reach of future experiments. Ongoing observations by *Fermi*, HESS, VERITAS, and MAGIC and future observations by the planned CTA and AGIS experiments will continue to improve the prospects for detecting and mapping a dark matter signal in the coming years.

Acknowledgments

We thank Joakim Edsjö and Torbjörn Sojstrand for help with PYTHIA and Jorge Peñarrubia for useful communications. SPR thanks the CCAPP, where this work started, and JSG thanks the CFTP for hospitality. SPR is partially supported by the Portuguese FCT through CERN/FP/83503/2008, CERN/FP/109305/2009 and CFTP-FCT UNIT 777, which are partially funded through POCTI (FEDER), and by the

Spanish Grant FPA2008-02878 of the MICINN. JSG acknowledges partial support from NSF CAREER Grant PHY-0547102 (to John Beacom).

References

- [1] G. Jungman, M. Kamionkowski and K. Griest, Phys. Rept. **267**, 195 (1996) [arXiv:hep-ph/9506380];
- [2] L. Bergstrom, Rept. Prog. Phys. **63**, 793 (2000) [arXiv:hep-ph/0002126];
- [3] G. Bertone, D. Hooper and J. Silk, Phys. Rept. **405**, 279 (2005) [arXiv:hep-ph/0404175].
- [4] J. Dunkley *et al.* [WMAP Collaboration], Astrophys. J. Suppl. **180**, 306 (2009) [arXiv:0803.0586 [astro-ph]].
- [5] L. Bergstrom, New J. Phys. **11**, 105006 (2009) [arXiv:0903.4849 [hep-ph]].
- [6] J. Preskill, M. B. Wise and F. Wilczek, Phys. Lett. B **120**, 127 (1983); L. F. Abbott and P. Sikivie, Phys. Lett. B **120**, 133 (1983); M. Dine and W. Fischler, Phys. Lett. B **120**, 137 (1983).
- [7] S. Dodelson and L. M. Widrow, Phys. Rev. Lett. **72**, 17 (1994) [arXiv:hep-ph/9303287].
- [8] C. Boehm and P. Fayet, Nucl. Phys. B **683**, 219 (2004) [arXiv:hep-ph/0305261]; C. Boehm, P. Fayet and J. Silk, Phys. Rev. D **69**, 101302(R) (2004) [arXiv:hep-ph/0311143].
- [9] C. Boehm, D. Hooper, J. Silk, M. Casse and J. Paul, Phys. Rev. Lett. **92**, 101301 (2004) [arXiv:astro-ph/0309686].
- [10] D. Hooper, F. Ferrer, C. Boehm, J. Silk, J. Paul, N. W. Evans and M. Casse, Phys. Rev. Lett. **93**, 161302 (2004) [arXiv:astro-ph/0311150]; C. Boehm and J. Silk, Phys. Lett. B **661**, 287 (2008) [arXiv:0708.2768 [hep-ph]].
- [11] C. Boehm, Y. Farzan, T. Hambye, S. Palomares-Ruiz and S. Pascoli, Phys. Rev. D **77**, 043516 (2008) [arXiv:hep-ph/0612228].
- [12] A. Birkedal, A. Noble, M. Perelstein and A. Spray, Phys. Rev. D **74**, 035002 (2006) [arXiv:hep-ph/0603077].
- [13] D. Hooper and S. Profumo, Phys. Rept. **453**, 29 (2007) [arXiv:hep-ph/0701197].
- [14] M. Kaplinghat, L. Knox and M. S. Turner, Phys. Rev. Lett. **85**, 3335 (2000) [arXiv:astro-ph/0005210].
- [15] K. Griest and M. Kamionkowski, Phys. Rev. Lett. **64**, 615 (1990); L. Hui, Phys. Rev. Lett. **86**, 3467 (2001) [arXiv:astro-ph/0102349].
- [16] M. S. Turner, G. Steigman and L. M. Krauss, Phys. Rev. Lett. **52**, 2090 (1984); R. J. Scherrer and M. S. Turner, Phys. Rev. D **31**, 681 (1985); M. S. Turner, Phys. Rev. D **31**, 1212 (1985); K. A. Olive and J. Silk, Phys. Rev. Lett. **55**, 2362 (1985); L. M. Krauss, Gen. Rel. Grav. **17**, 89 (1985); D. A. Dicus and V. L. Teplitz, Phys. Rev. D **34**, 934 (1986); A. Dekel and T. Piran, Astrophys. J. **315**, L83 (1987); D. W. Sciama, Astrophys. J. **364**, 549 (1990); R. Cen, Astrophys. J. **546**, L77 (2001) [arXiv:astro-ph/0005206]; R. Cen, Astrophys. J. **549**, L195 (2001) [arXiv:astro-ph/0012051]; K. Ichiki, P. M. Garnavich, T. Kajino, G. J. Mathews and M. Yahiro, Phys. Rev. D **68**, 083518 (2003) [arXiv:astro-ph/0210052]; F. J. Sanchez-Salcedo, Astrophys. J. **591**, L107 (2003) [arXiv:astro-ph/0305496]; M. Oguri, K. Takahashi, H. Ohno and K. Kotake, Astrophys. J. **597**, 645 (2003) [arXiv:astro-ph/0306020]; X. L. Chen and M. Kamionkowski, Phys. Rev. D **70**, 043502 (2004) [arXiv:astro-ph/0310473]; K. Takahashi, M. Oguri and K. Ichiki, Mon. Not. Roy. Astron. Soc. **352**, 311 (2004) [arXiv:astro-ph/0312358]; D. Hooper and L. T. Wang, Phys. Rev. D **70**, 063506 (2004) [arXiv:hep-ph/0402220]; M. Mapelli, A. Ferrara and E. Pierpaoli, Mon. Not. Roy. Astron. Soc. **369**, 1719 (2006) [arXiv:astro-ph/0603237]; L. M. Krauss and R. J. Scherrer, Phys. Rev. D **75**, 083524 (2007) [arXiv:astro-ph/0702207]; J. A. R. Cembranos, J. L. Feng and L. E. Strigari, Phys. Rev. Lett. **99**, 191301 (2007) [arXiv:0704.1658 [astro-ph]]; M. Lattanzi and J. W. F. Valle, Phys. Rev. Lett. **99**, 121301 (2007) [arXiv:0705.2406 [astro-ph]]; M. Abdelqader and F. Melia, Mon. Not. Roy. Astron. Soc. **388**, 1869 (2008) [arXiv:0806.0602 [astro-ph]]; F. Ferrer, C. Nipoti and S. Etori, Phys. Rev. D **80**, 061303 (2009) [arXiv:0905.3161 [astro-ph.CO]].

- [17] O. Adriani *et al.* [PAMELA Collaboration], *Nature* **458**, 607 (2009) [arXiv:0810.4995 [astro-ph]]; O. Adriani *et al.* [PAMELA Collaboration], *Astropart. Phys.* **34**, 1 (2010) [arXiv:1001.3522 [astro-ph.HE]].
- [18] M. Cirelli, M. Kadastik, M. Raidal and A. Strumia, *Nucl. Phys. B* **813**, 1 (2009) [arXiv:0809.2409 [hep-ph]].
- [19] V. Barger, W. Y. Keung, D. Marfatia and G. Shaughnessy, *Phys. Lett. B* **672**, 141 (2009) [arXiv:0809.0162 [hep-ph]].
- [20] N. Arkani-Hamed, D. P. Finkbeiner, T. R. Slatyer and N. Weiner, *Phys. Rev. D* **79**, 015014 (2009) [arXiv:0810.0713 [hep-ph]]; M. Pospelov and A. Ritz, *Phys. Lett. B* **671**, 391 (2009) [arXiv:0810.1502 [hep-ph]]; I. Cholis, D. P. Finkbeiner, L. Goodenough and N. Weiner, *JCAP* **0912**, 007 (2009) [arXiv:0810.5344 [astro-ph]]; Y. Nomura and J. Thaler, *Phys. Rev. D* **79**, 075008 (2009) [arXiv:0810.5397 [hep-ph]]; R. Harnik and G. D. Kribs, *Phys. Rev. D* **79**, 095007 (2009) [arXiv:0810.5557 [hep-ph]]; D. Feldman, Z. Liu and P. Nath, *Phys. Rev. D* **79**, 063509 (2009) [arXiv:0810.5762 [hep-ph]]; I. Cholis, G. Dobler, D. P. Finkbeiner, L. Goodenough and N. Weiner, *Phys. Rev. D* **80**, 123518 (2009) [arXiv:0811.3641 [astro-ph]]; P. J. Fox and E. Poppitz, *Phys. Rev. D* **79**, 083528 (2009) [arXiv:0811.0399 [hep-ph]]; R. Allahverdi, B. Dutta, K. Richardson-McDaniel and Y. Santoso, *Phys. Rev. D* **79**, 075005 (2009) [arXiv:0812.2196 [hep-ph]].
- [21] D. Grasso *et al.* [Fermi-LAT Collaboration], *Astropart. Phys.* **32**, 140 (2009) [arXiv:0905.0636 [astro-ph.HE]].
- [22] P. f. Yin, Q. Yuan, J. Liu, J. Zhang, X. j. Bi and S. h. Zhu, *Phys. Rev. D* **79**, 023512 (2009) [arXiv:0811.0176 [hep-ph]]; C. R. Chen, F. Takahashi and T. T. Yanagida, *Phys. Lett. B* **673**, 255 (2009) [arXiv:0811.0477 [hep-ph]]; K. Hamaguchi, E. Nakamura, S. Shirai and T. T. Yanagida, *Phys. Lett. B* **674**, 299 (2009) [arXiv:0811.0737 [hep-ph]]; A. Ibarra and D. Tran, *JCAP* **0902**, 021 (2009) [arXiv:0811.1555 [hep-ph]]; C. R. Chen, M. M. Nojiri, F. Takahashi and T. T. Yanagida, *Prog. Theor. Phys.* **122**, 553 (2009) [arXiv:0811.3357 [astro-ph]].
- [23] E. Nardi, F. Sannino and A. Strumia, *JCAP* **0901**, 043 (2009) [arXiv:0811.4153 [hep-ph]].
- [24] K. Cheung, P. Y. Tseng and T. C. Yuan, *Phys. Lett. B* **678**, 293 (2009) [arXiv:0902.4035 [hep-ph]].
- [25] X. G. He, *Mod. Phys. Lett. A* **52**, 2139 (2009) [arXiv:0908.2908 [hep-ph]].
- [26] P. Brun, T. Delahaye, J. Diemand, S. Profumo and P. Salati, *Phys. Rev. D* **80**, 035023 (2009) [arXiv:0904.0812 [astro-ph.HE]].
- [27] J. M. Cline, A. C. Vincent and W. Xue, *Phys. Rev. D* **81**, 083512 (2010) [arXiv:1001.5399 [astro-ph.CO]].
- [28] C. Rott [IceCube Collaboration], arXiv:0912.5183 [astro-ph.HE].
- [29] R. Abbasi *et al.* [IceCube Collaboration], *Phys. Rev. Lett.* **102**, 201302 (2009) [arXiv:0902.2460 [astro-ph.CO]]; G. Wikstrom and J. Edsjo, *JCAP* **0904**, 009 (2009) [arXiv:0903.2986 [astro-ph.CO]]; R. Abbasi *et al.* [IceCube Collaboration], *Phys. Rev. D* **81**, 057101 (2010) [arXiv:0910.4480 [astro-ph.CO]]; F. Halzen and D. Hooper, *New J. Phys.* **11**, 105019 (2009) [arXiv:0910.4513 [astro-ph.HE]].
- [30] L. Bergstrom, J. Edsjo and P. Ullio, *Phys. Rev. Lett.* **87**, 251301 (2001) [arXiv:astro-ph/0105048]; P. Ullio, L. Bergstrom, J. Edsjo and C. G. Lacey, *Phys. Rev. D* **66**, 123502 (2002) [arXiv:astro-ph/0207125]; L. Pieri and E. Branchini, *Phys. Rev. D* **69**, 043512 (2004) [arXiv:astro-ph/0307209]; A. V. Belikov and D. Hooper, *Phys. Rev. D* **81**, 043505 (2010) [arXiv:0906.2251 [astro-ph.CO]]; S. Profumo and T. E. Jeltema, *JCAP* **0907**, 020 (2009) [arXiv:0906.0001 [astro-ph.CO]]; M. Pohl and D. Eichler, *Astrophys. J. Lett.* **712**, L53 (2010) [arXiv:0912.1203 [astro-ph.HE]]; K. N. Abazajian, P. Agrawal, Z. Chacko and C. Kilic, arXiv:1002.3820 [astro-ph.HE].
- [31] V. S. Berezinsky, A. V. Gurevich and K. P. Zybin, *Phys. Lett. B* **294**, 221 (1992); V. Berezinsky, A. Bottino and G. Mignola, *Phys. Lett. B* **325**, 136 (1994) [arXiv:hep-ph/9402215]; L. Bergstrom, P. Ullio and J. H. Buckley, *Astropart. Phys.* **9**, 137 (1998) [arXiv:astro-ph/9712318]; A. Cesarini, F. Fucito, A. Lionetto, A. Morselli and P. Ullio, *Astropart. Phys.* **21**, 267 (2004) [arXiv:astro-ph/0305075].

- [32] J. Albert *et al.* [MAGIC Collaboration], *Astrophys. J.* **638**, L101 (2006) [arXiv:astro-ph/0512469].
- [33] F. Aharonian *et al.* [HESS Collaboration], *Phys. Rev. Lett.* **97**, 221102 (2006) [Erratum-ibid. **97**, 249901 (2006)] [arXiv:astro-ph/0610509].
- [34] E. A. Baltz *et al.*, *JCAP* **0807**, 013 (2008) [arXiv:0806.2911 [astro-ph]].
- [35] C. Calcano-Roldan and B. Moore, *Phys. Rev. D* **62**, 123005 (2000) [arXiv:astro-ph/0010056]; F. Stoehr, S. D. M. White, V. Springel, G. Tormen and N. Yoshida, *Mon. Not. Roy. Astron. Soc.* **345**, 1313 (2003) [arXiv:astro-ph/0307026]; V. Springel *et al.*, *Nature* **456N7218**, 73 (2008).
- [36] L. Pieri, J. Lavalle, G. Bertone and E. Branchini, arXiv:0908.0195 [astro-ph.HE].
- [37] A. A. Abdo *et al.*, *Phys. Rev. Lett.* **104**, 091302 (2010) [arXiv:1001.4836 [astro-ph.HE]].
- [38] A. Tasitsiomi and A. V. Olinto, *Phys. Rev. D* **66**, 083006 (2002) [arXiv:astro-ph/0206040]; S. M. Koushiappas, A. R. Zentner and T. P. Walker, *Phys. Rev. D* **69**, 043501 (2004) [arXiv:astro-ph/0309464]; L. Pieri, E. Branchini and S. Hofmann, *Phys. Rev. Lett.* **95**, 211301 (2005) [arXiv:astro-ph/0505356]; S. M. Koushiappas, *Phys. Rev. Lett.* **97**, 191301 (2006) [arXiv:astro-ph/0606208]; L. Pieri, G. Bertone and E. Branchini, *Mon. Not. Roy. Astron. Soc.* **384**, 1627 (2008) [arXiv:0706.2101 [astro-ph]]. J. Diemand, M. Kuhlen and P. Madau, *Astrophys. J.* **657**, 262 (2007) [arXiv:astro-ph/0611370];
- [39] M. Kuhlen, J. Diemand and P. Madau, *Astrophys. J.* **686**, 262 (2008) [arXiv:0805.4416 [astro-ph]].
- [40] E. A. Baltz, C. Briot, P. Salati, R. Taillet and J. Silk, *Phys. Rev. D* **61**, 023514 (2000) [arXiv:astro-ph/9909112]; C. Tyler, *Phys. Rev. D* **66**, 023509 (2002) [arXiv:astro-ph/0203242]; A. Tasitsiomi, J. M. Siegal-Gaskins and A. V. Olinto, *Astropart. Phys.* **21**, 637 (2004) [arXiv:astro-ph/0307375]; L. Bergstrom and D. Hooper, *Phys. Rev. D* **73**, 063510 (2006) [arXiv:hep-ph/0512317]; L. E. Strigari, S. M. Koushiappas, J. S. Bullock and M. Kaplinghat, *Phys. Rev. D* **75**, 083526 (2007) [arXiv:astro-ph/0611925]; T. Bringmann, M. Doro and M. Fornasa, *JCAP* **0901**, 016 (2009) [arXiv:0809.2269 [astro-ph]]; L. Pieri, A. Pizzella, E. M. Corsini, E. D. Bonta' and F. Bertola, *Astron. Astrophys.* **496**, 351 (2009) [arXiv:0812.1494 [astro-ph]]; G. D. Martinez, J. S. Bullock, M. Kaplinghat, L. E. Strigari and R. Trotta, *JCAP* **0906**, 014 (2009) [arXiv:0902.4715 [astro-ph.HE]]; P. Scott, J. Conrad, J. Edsjo, L. Bergstrom, C. Farnier and Y. Akrami, *JCAP* **1001**, 031 (2010) [arXiv:0909.3300 [astro-ph.CO]].
- [41] N. W. Evans, F. Ferrer and S. Sarkar, *Phys. Rev. D* **69**, 123501 (2004) [arXiv:astro-ph/0311145].
- [42] L. E. Strigari, S. M. Koushiappas, J. S. Bullock, M. Kaplinghat, J. D. Simon, M. Geha and B. Willman, *Astrophys. J.* **678**, 614 (2008) [arXiv:0709.1510 [astro-ph]].
- [43] R. Essig, N. Sehgal and L. E. Strigari, *Phys. Rev. D* **80**, 023506 (2009) [arXiv:0902.4750 [hep-ph]].
- [44] J. Albert *et al.* [MAGIC Collaboration], *Astrophys. J.* **679**, 428 (2008) [arXiv:0711.2574 [astro-ph]]; E. Aliu *et al.* [MAGIC Collaboration], *Astrophys. J.* **697**, 1299 (2009) [arXiv:0810.3561 [astro-ph]]; S. Lombardi *et al.* [MAGIC Collaboration], arXiv:0907.0738 [astro-ph.HE].
- [45] F. Aharonian [HESS Collaboration], *Astropart. Phys.* **29**, 55 (2008) [arXiv:0711.2369 [astro-ph]]; F. Aharonian [HESS Collaboration], *Astrophys. J.* **691**, 175 (2009) [arXiv:0809.3894 [astro-ph]]; E. Moulin [HESS Collaboration], *AIP Conf. Proc.* **1166**, 179 (2009).
- [46] D. D. Driscoll *et al.*, *Phys. Rev. D* **78**, 087101 (2008).
- [47] R. G. Wagner [VERITAS Collaboration], arXiv:0910.4563 [astro-ph.HE].
- [48] A. A. Abdo *et al.* [Fermi-LAT Collaboration], *Astrophys. J.* **712**, 147 (2010) [arXiv:1001.4531 [astro-ph.CO]].
- [49] J. D. Lewin and P. F. Smith, *Astropart. Phys.* **6**, 87 (1996); A. M. Green, *JCAP* **0708**, 022 (2007) [arXiv:hep-ph/0703217]; G. Bertone, D. G. Cerdeno, J. I. Collar and B. C. Odom, *Phys. Rev. Lett.* **99**, 151301 (2007) [arXiv:0705.2502 [astro-ph]]; C. L. Shan and M. Drees, arXiv:0710.4296 [hep-ph]; M. Drees and C. L. Shan, *JCAP* **0806**, 012 (2008) [arXiv:0803.4477 [hep-ph]]; N. Bernal, A. Goudelis, Y. Mambrini and C. Muñoz, *JCAP* **0901**, 046 (2009) [arXiv:0804.1976 [hep-ph]]; A. M. Green, *JCAP* **0807**, 005 (2008) [arXiv:0805.1704 [hep-ph]]; C. L. Shan, *New J. Phys.* **11**, 105013 (2009) [arXiv:0903.4320 [hep-ph]]; Y. T. Chou and C. L. Shan, *JCAP* **1008**, 014 (2010) [arXiv:1003.5277 [hep-ph]].
- [50] J. Edsjo and P. Gondolo, *Phys. Lett. B* **357**, 595 (1995) [arXiv:hep-ph/9504283]; M. Cirelli,

- N. Fornengo, T. Montaruli, I. Sokalski, A. Strumia and F. Vissani, Nucl. Phys. B **727**, 99 (2005) [Erratum-ibid. B **790**, 338 (2008)] [arXiv:hep-ph/0506298]; O. Mena, S. Palomares-Ruiz and S. Pascoli, Phys. Lett. B **664**, 92 (2008) [arXiv:0706.3909 [hep-ph]].
- [51] S. Dodelson, D. Hooper and P. D. Serpico, Phys. Rev. D **77**, 063512 (2008) [arXiv:0711.4621 [astro-ph]]; T. E. Jeltema and S. Profumo, JCAP **0811**, 003 (2008) [arXiv:0808.2641 [astro-ph]]; N. Bernal and S. Palomares-Ruiz, arXiv:1006.0477 [astro-ph.HE].
- [52] B. S. Hensley, J. M. Siegal-Gaskins and V. Pavlidou, arXiv:0912.1854 [astro-ph.CO].
- [53] M. Beltran, D. Hooper, E. W. Kolb and Z. C. Krusberg, Phys. Rev. D **80**, 043509 (2009) [arXiv:0808.3384 [hep-ph]].
- [54] W. B. Atwood *et al.* [Fermi-LAT Collaboration], Astrophys. J. **697**, 1071 (2009) [arXiv:0902.1089 [astro-ph.IM]].
- [55] J. A. Hinton [HESS Collaboration], New Astron. Rev. **48**, 331 (2004) [arXiv:astro-ph/0403052].
- [56] J. Holder *et al.*, AIP Conf. Proc. **1085**, 657 (2009) [arXiv:0810.0474 [astro-ph]].
- [57] E. Lorenz [MAGIC Collaboration], New Astron. Rev. **48**, 339 (2004).
- [58] R. M. Wagner, E. J. Lindfors, A. Sillanpaa, S. Wagner [CTA Consortium], arXiv:0912.3742 [astro-ph.IM].
- [59] J. Buckley *et al.* [AGIS Collaboration], AIP Conf. Proc. **1085**, 902 (2009).
- [60] G. Bertone, W. Buchmuller, L. Covi and A. Ibarra, JCAP **0711**, 003 (2007) [arXiv:0709.2299 [astro-ph]].
- [61] S. Palomares-Ruiz, Phys. Lett. B **665**, 50 (2008) [arXiv:0712.1937 [astro-ph]].
- [62] J. D. Simon and M. Geha, Astrophys. J. **670**, 313 (2007) [arXiv:0706.0516 [astro-ph]].
- [63] N. F. Martin, J. T. A. de Jong and H. W. A. Rix, Astrophys. J. **684**, 1075 (2008) [arXiv:0805.2945 [astro-ph]].
- [64] E. A. Baltz and L. Wai, Phys. Rev. D **70**, 023512 (2004) [arXiv:astro-ph/0403528].
- [65] T. E. Jeltema and S. Profumo, Astrophys. J. **686**, 1045 (2008) [arXiv:0805.1054 [astro-ph]].
- [66] M. Kuhlen, Adv. Astron. 2010, 162083 [arXiv:0906.1822 [astro-ph.GA]].
- [67] M. D. Kistler and J. M. Siegal-Gaskins, Phys. Rev. D **81**, 103521 (2010) [arXiv:0909.0519 [astro-ph.HE]].
- [68] J. Diemand, M. Kuhlen, P. Madau, M. Zemp, B. Moore, D. Potter and J. Stadel, Nature **454**, 735 (2008). [arXiv:0805.1244 [astro-ph]].
- [69] V. Springel *et al.*, Mon. Not. Roy. Astron. Soc. **391**, 1685 (2008) [arXiv:0809.0898 [astro-ph]].
- [70] J. Diemand, M. Kuhlen and P. Madau, Astrophys. J. **667**, 859 (2007) [arXiv:astro-ph/0703337]; L. E. Strigari, J. S. Bullock, M. Kaplinghat, J. Diemand, M. Kuhlen and P. Madau, Astrophys. J. **669**, 676 (2007) [arXiv:0704.1817 [astro-ph]]; P. Madau, J. Diemand and M. Kuhlen, Astrophys. J. **679**, 1260 (2008) [arXiv:0802.2265 [astro-ph]]; T. Okamoto and C. S. Frenk, Mon. Not. Roy. Astron. Soc. **399**, L174 (2009) [arXiv:0909.0262 [astro-ph.CO]].
- [71] E. Hayashi, J. F. Navarro, J. E. Taylor, J. Stadel and T. R. Quinn, Astrophys. J. **584**, 541 (2003) [arXiv:astro-ph/0203004].
- [72] S. Kazantzidis, L. Mayer, C. Mastropietro, J. Diemand, J. Stadel and B. Moore, Astrophys. J. **608**, 663 (2004) [arXiv:astro-ph/0312194].
- [73] J. Penarrubia, J. F. Navarro and A. W. McConnachie, Astrophys. J. **673**, 226 (2008) [arXiv:0708.3087 [astro-ph]].
- [74] M. G. Walker, M. Mateo, E. W. Olszewski, J. Penarrubia, N. W. Evans and G. Gilmore, Astrophys. J. **704**, 1274 (2009) [Erratum-ibid. **710**, 886 (2010)] [arXiv:0906.0341 [astro-ph.CO]].
- [75] J. F. Navarro, C. S. Frenk and S. D. M. White, Mon. Not. Roy. Astron. Soc. **275**, 720 (1995) [arXiv:astro-ph/9408069]; J. F. Navarro, C. S. Frenk and S. D. M. White, Astrophys. J. **462**, 563 (1996) [arXiv:astro-ph/9508025]; J. F. Navarro, C. S. Frenk and S. D. M. White, Astrophys. J. **490**, 493 (1997) [arXiv:astro-ph/9611107].
- [76] L. E. Strigari, J. S. Bullock, M. Kaplinghat, J. D. Simon, M. Geha, B. Willman and M. G. Walker, Nature **454**, 1096 (2008) [arXiv:0808.3772 [astro-ph]].
- [77] A. Z. Bonanos, K. Z. Stanek, A. H. Szentgyorgyi, D. D. Sasselov and G. A. Bakos, Astron. J. **127**,

- 861 (2004) [Erratum-ibid. **133**, 756 (2007)] [arXiv:astro-ph/0310477].
- [78] M. Mateo, *Ann. Rev. Astron. Astrophys.* **36** (1998) 435 [arXiv:astro-ph/9810070].
- [79] J. Einasto, *Trudy Inst. Astroz. Alma-Ata*, **5**, 87 (1965).
- [80] J. Mardon, Y. Nomura, D. Stolarski and J. Thaler, *JCAP* **0905**, 016 (2009) [arXiv:0901.2926 [hep-ph]]; F. Chen, J. M. Cline and A. R. Frey, *Phys. Rev. D* **79**, 063530 (2009) [arXiv:0901.4327 [hep-ph]]; I. Z. Rothstein, T. Schwetz and J. Zupan, *JCAP* **0907**, 018 (2009) [arXiv:0903.3116 [astro-ph.HE]].
- [81] P. Meade, M. Papucci, A. Strumia and T. Volansky, *Nucl. Phys. B* **831**, 178 (2010) [arXiv:0905.0480 [hep-ph]].
- [82] M. Papucci and A. Strumia, *JCAP* **1003**, 014 (2010) [arXiv:0912.0742 [hep-ph]].
- [83] T. Sjostrand, S. Mrenna and P. Skands, *JHEP* **0605**, 026 (2006) [arXiv:hep-ph/0603175].
- [84] M. Cirelli, P. Panci and P. D. Serpico, arXiv:0912.0663 [astro-ph.CO].
- [85] C. R. Chen, S. K. Mandal and F. Takahashi, *JCAP* **1001**, 023 (2010) [arXiv:0910.2639 [hep-ph]].
- [86] L. Zhang, C. Weniger, L. Maccione, J. Redondo and G. Sigl, *JCAP* **1006**, 027 (2010) [arXiv:0912.4504 [astro-ph.HE]].
- [87] R. Barbieri and V. Berezhinsky, *Phys. Lett. B* **205**, 559 (1988); M. Kamionkowski, arXiv:astro-ph/9404079; G. D. Kribs and I. Z. Rothstein, *Phys. Rev. D* **55**, 4435 (1997) [Erratum-ibid. *D* **56**, 1822 (1997)] [arXiv:hep-ph/9610468]; H. B. Kim and J. E. Kim, *Phys. Lett. B* **527**, 18 (2002) [arXiv:hep-ph/0108101]; L. Zhang, X. Chen, M. Kamionkowski, Z. G. Si and Z. Zheng, *Phys. Rev. D* **76**, 061301(R) (2007) [arXiv:0704.2444 [astro-ph]]; H. Yuksel and M. D. Kistler, *Phys. Rev. D* **78**, 023502 (2008) [arXiv:0711.2906 [astro-ph]]; G. D. Mack, T. D. Jacques, J. F. Beacom, N. F. Bell and H. Yuksel, *Phys. Rev. D* **78**, 063542 (2008) [arXiv:0803.0157 [astro-ph]].
- [88] K. Ichiki, M. Oguri and K. Takahashi, *Phys. Rev. Lett.* **93**, 071302 (2004) [arXiv:astro-ph/0403164]; Y. Gong and X. Chen, *Phys. Rev. D* **77**, 103511 (2008) [arXiv:0802.2296 [astro-ph]]; S. De Lope Amigo, W. Y. Cheung, Z. Huang and S. P. Ng, *JCAP* **0906**, 005 (2009) [arXiv:0812.4016 [hep-ph]].
- [89] M. Kachelriess and P. D. Serpico, *Phys. Rev. D* **76**, 063516 (2007) [arXiv:0707.0209 [hep-ph]]; M. Regis and P. Ullio, *Phys. Rev. D* **78**, 043505 (2008) [arXiv:0802.0234 [hep-ph]]; N. F. Bell, J. B. Dent, T. D. Jacques and T. J. Weiler, *Phys. Rev. D* **78**, 083540 (2008) [arXiv:0805.3423 [hep-ph]]; J. B. Dent, R. J. Scherrer and T. J. Weiler, *Phys. Rev. D* **78**, 063509 (2008) [arXiv:0806.0370 [astro-ph]]; E. Borriello, A. Cuoco and G. Miele, *Phys. Rev. D* **79**, 023518 (2009) [arXiv:0809.2990 [astro-ph]]; G. Bertone, M. Cirelli, A. Strumia and M. Taoso, *JCAP* **0903**, 009 (2009) [arXiv:0811.3744 [astro-ph]]; M. Cirelli and P. Panci, *Nucl. Phys. B* **821**, 399 (2009) [arXiv:0904.3830 [astro-ph.CO]]; M. Kachelriess, P. D. Serpico and M. A. Solberg, *Phys. Rev. D* **80**, 123533 (2009) [arXiv:0911.0001 [hep-ph]]; T. Bringmann, arXiv:0911.1124 [hep-ph]; R. M. Crocker, N. F. Bell, C. Balazs and D. I. Jones, *Phys. Rev. D* **81**, 063516 (2010) [arXiv:1002.0229 [hep-ph]].
- [90] J. F. Beacom, N. F. Bell and G. D. Mack, *Phys. Rev. Lett.* **99**, 231301 (2007) [arXiv:astro-ph/0608090]; H. Yuksel, S. Horiuchi, J. F. Beacom and S. Ando, *Phys. Rev. D* **76**, 123506 (2007) [arXiv:0707.0196 [astro-ph]]; S. Palomares-Ruiz and S. Pascoli, *Phys. Rev. D* **77**, 025025 (2008) [arXiv:0710.5420 [astro-ph]].
- [91] S. Galli, F. Iocco, G. Bertone and A. Melchiorri, *Phys. Rev. D* **80**, 023505 (2009) [arXiv:0905.0003 [astro-ph.CO]]; G. Huetsi, A. Hektor and M. Raidal, *Astron. Astrophys.* **505**, 999 (2009) [arXiv:0906.4550 [astro-ph.CO]]; M. Cirelli, F. Iocco and P. Panci, *JCAP* **0910**, 009 (2009) [arXiv:0907.0719 [astro-ph.CO]]; T. R. Slatyer, N. Padmanabhan and D. P. Finkbeiner, *Phys. Rev. D* **80**, 043526 (2009) [arXiv:0906.1197 [astro-ph.CO]].
- [92] C. Boehm, T. Delahaye and J. Silk, arXiv:1003.1225 [astro-ph.GA].